

1 Triassic – Jurassic salt movement in the Baltic sector of the North
2 German Basin and its relation to post-Permian regional tectonics
3

4 Niklas Ahlrichs^{1,2}, Vera Noack¹, Elisabeth Seidel², Christian Hübscher²

5 ¹Federal Institute for Geosciences and Natural Resources (BGR), Berlin Branch Office, Berlin,
6 Germany.

7 ²Institute of Geophysics, Center for Earth System Research and Sustainability, Universität Hamburg,
8 Hamburg, Germany.

9 Corresponding author: Niklas Ahlrichs:

10 Mail: niklas.ahlrichs@uni-hamburg.de, vera.noack@bgr.de, Elisabeth.seidel@uni-hamburg.de,
11 christian.huebscher@uni-hamburg.de

12

13 This manuscript has been submitted for publication at the journal *Basin Research*. The manuscript
14 has undergone peer review represents the revised and resubmitted version of the manuscript.
15 Subsequent versions may have slightly different content due to the ongoing review process. When
16 accepted, the final version of the manuscript will be available via the peer reviewed publication DOI
17 link.

18

19

20 Triassic – Jurassic salt movement in the Baltic sector of the North 21 German Basin and its relation to post-Permian regional tectonics

22

23 Niklas Ahlrichs^{1,2}, Vera Noack¹, Elisabeth Seidel², Christian Hübscher²

24 ¹Federal Institute for Geosciences and Natural Resources (BGR), Berlin Branch Office, Berlin,
25 Germany.

26 ²Institute of Geophysics, Center for Earth System Research and Sustainability, Universität Hamburg,
27 Hamburg, Germany.

28 Corresponding author: Niklas Ahlrichs:

29

30 Abstract

31 The formation and structural evolution of complex intracontinental basins, like the North German
32 Basin, mark fundamental earth processes. Understanding these is not only essential to basic research
33 but also of socioeconomic importance because of its multitude of resources, potential hazards and
34 subsurface use capability. As part of the Central European Basin System, major subsidence and
35 structural differentiation affected the Baltic sector of the North German Basin in Permian to Jurassic
36 times. A dense network of high-resolution 2D seismic data together with nearby wells allow creating
37 regional maps with refined stratigraphic subdivision of unprecedented spatial resolution covering the
38 bays of Kiel and Mecklenburg. Cross sections covering the basin margin allow reconstructing the
39 structural evolution of the Zechstein salt and its overburden. At the northern basin margin, near the
40 Kegnaes Diapir, thinning of the Buntsandstein and divergent reflectors indicate an Early Triassic stage
41 of faulting and salt movement, which suggests that the common concept of relatively quiet tectonic
42 conditions during Early Triassic thermal subsidence would have to be expanded. In the Late Triassic,
43 tectonic activity increased as expressed by the onset of salt movement in the northeastern
44 Glückstadt Graben, major growth of the Kegnaes Diapir and faulting at the northeastern basin margin
45 during deposition of the Keuper (Erfurt, Grabfeld, Stuttgart and Weser formations). We explain the
46 pillow to diapir transition of the Kegnaes Diapir by extension and erosional unroofing during the Late
47 Triassic. At the northeastern basin margin, we interpret the accumulation of Keuper and Jurassic
48 deposits as an infill of a transtensional sub-basin. This area, bordered by the Werre Fault Zone and
49 Agricola Fault System, forms the northwestern prolongation of the Western Pomeranian Fault
50 System. Between the Glückstadt Graben and the northeastern basin margin, the Eastholstein-
51 Mecklenburg Block formed a more stable area, where salt movement first began during the latest
52 Triassic.

53 1. Introduction

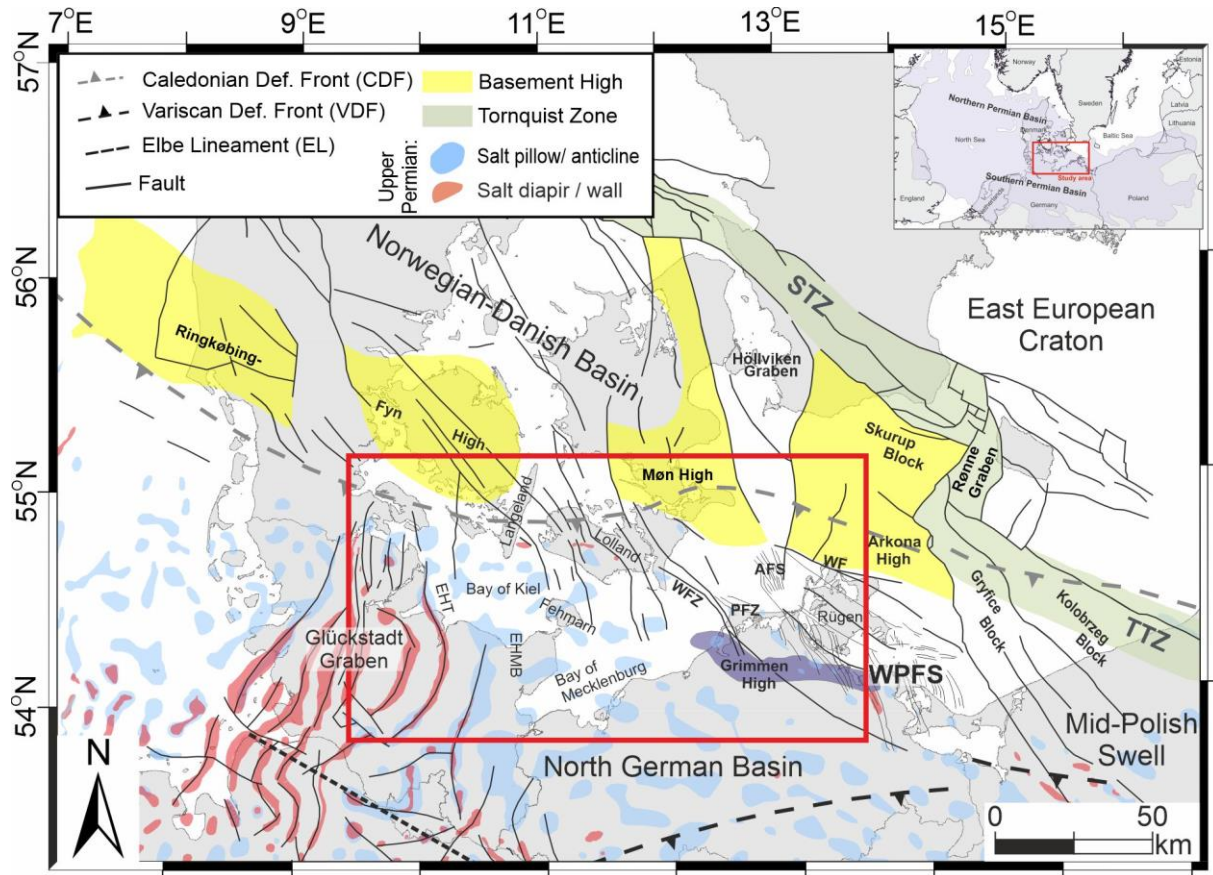
54 The North German Basin forms part of the intracontinental Southern Permian Basin and has a
55 complex and long history of basin evolution from the Carboniferous to Quaternary (Fig. 1) (see e.g.
56 overviews: Ziegler, 1990a; Maystrenko et al., 2008; Pharaoh et al., 2010). Even though the overall
57 basin evolution is well understood, the link between regional tectonics, salt movement and inherited
58 deep-rooted structures at a regional scale and the temporal resolution of geological stages remains
59 partly elusive. In times of growing interest in the usage of the deeper subsurface, e.g. for
60 geoengineering projects like Carbon Capture and Storage (CCS), geothermal energy utilization,
61 storage of renewable energy or the search for a nuclear repository, a profound understanding of the
62 evolution of the basin and its deep-rooted fault systems is very important (Gill, 2017).

63 The Baltic sector of the North German Basin (NGB) covers the northern basin margin including a part
64 of the northeastern Glückstadt Graben, which experienced intensive extension and salt movement
65 during the Triassic, and the Western Pomeranian Fault System at the northeastern basin margin,
66 which developed due to Triassic transtensional tectonics (Fig. 1) (Krauss & Mayer, 2004; Maystrenko
67 et al., 2005a, 2005b). Many salt structures spread across the entire area making the Baltic sector of
68 the NGB an ideal study area to investigate the impact of regional tectonics on salt movement
69 (Vejbæk, 1997; Reinhold et al., 2008). Among the salt structures in the study area are a WNW-ESE
70 striking set of four salt diapirs at the northern basin margin, spreading across the island of Lolland
71 towards Langeland (Fig. 1). Their isolated location at the basin margin, surrounded by salt pillows, is
72 unique within the NGB. The causative relation of salt tectonics, basin configuration and regional
73 tectonics, which led to the formation of these diapirs, remains unclear.

74 In the past, much research analyzing the post Permian sedimentary record has been done in the
75 Baltic sector of the NGB (Hübscher et al., 2004; Hansen et al., 2005; Maystrenko et al., 2005a, 2005b;
76 Hansen et al., 2007; Zöllner et al., 2008; Hübscher et al., 2010; Al Hseinat & Hübscher, 2014; Al
77 Hseinat et al., 2016; Kammann et al., 2016; Al Hseinat & Hübscher, 2017; Deutschmann et al., 2018;
78 Hübscher et al., 2019; Frahm et al., 2020; Huster et al., 2020; Schnabel et al., 2021). These studies
79 used seismic imaging and mapping of post-Permian units with a lithostratigraphic subdivision
80 representing a vertical resolution in the order of geological series to analyze the regional tectonic and
81 salt tectonic structural evolution. From this, four major post Permian tectonic phases important for
82 salt structure evolution were identified: (1) Late Triassic – Early Jurassic extension triggering initial
83 salt movement; (2) Regional erosion due to uplift originating from the Mid Jurassic North Sea Doming
84 event; (3) Late Cretaceous inversion and compressional reactivation of salt movement; (4)
85 Paleogene-Neogene reactivation of salt movement. In a recent study, Ahlrichs et al. (2021) presented
86 regional maps of the Baltic sector of the NGB with a refined stratigraphic subdivision of Late
87 Cretaceous and Cenozoic units specifying the onset of Late Cretaceous inversion and Paleogene salt
88 movement. For the Triassic, such regional maps resolving the stratigraphic subdivision beyond the
89 level of the main lithostratigraphic units of the Germanic Triassic are lacking in the Baltic sector of
90 the North German Basin. Studies carried out in the adjacent onshore areas (Denmark: Clausen &
91 Pedersen, 1999; Glückstadt Graben and Lower Saxony: Frisch & Kockel, 1999; Baldschuhn et al.,
92 2001; Kockel, 2002; Warsitzka et al., 2016; Mecklenburg-Western Pomerania: Beutler et al., 2012)
93 show a refined stratigraphic subdivision of the Triassic units. These authors specified that the onset
94 of extensional tectonics and initial salt movement in the Late Triassic occurred during deposition of
95 the Keuper (Grabfeld and Weser formations, Fig. 2).

96 In this study, we focus on the Triassic-Jurassic phase of basin evolution to enhance both the
97 understanding of regional tectonics and the initial development of salt structures prior to Late
98 Cretaceous inversion. We use a dense network of high-resolution 2D seismic data in combination
99 with onshore and offshore wells to refine the stratigraphic subdivision of the Triassic and create
100 regional maps of the Triassic - Jurassic units, which close the gap to adjacent onshore areas (Fig. 3).
101 We present key seismic profiles and regional time-structure and isochron maps of the Zechstein,
102 Buntsandstein, Muschelkalk, Keuper II (Erfurt, Grabfeld, Stuttgart, Weser formations), Keuper I
103 (Arnstadt, Exeter formations) and Jurassic units (mostly Liassic) to analyze the Triassic to Jurassic
104 structural evolution of the region (Fig. 2). Thereby, we strive for a detailed structural analysis of the
105 basin margin and its fault systems and propose an explanation for the development of salt diapirs at
106 the northern basin margin. Together with previous studies setting up the stratigraphic framework
107 (Ahlrichs et al., 2020) and investigating the Late Cretaceous and Cenozoic development (Ahlrichs et
108 al., 2021), this study completes the analysis of the impact of regional post-Permian tectonics on salt
109 structure evolution in the Baltic sector of the NGB. Additionally, our results contribute to a planned
110 offshore extension of the recently published 3D geological overview model of the onshore part of the

111 NGB, which was developed to meet the increasing demands on subsurface use in Germany (TUNB
 112 Working Group, 2021).



113
 114 *Figure 1: Structural overview of the northern North German Basin (modified after Ahlrichs et al., 2020; Ahlrichs et al., 2021).*
 115 *Inset shows approximate outline of the northern and southern Permian Basin (present day limit of Permian deposits after*
 116 *Maystrenko & Scheck-Wenderoth, 2013). Red box shows study area. Salt structures were compiled after Vejrbæk (1997);*
 117 *Dadlez and Marek (1998); Reinhold et al. (2008); Warsitzka et al. (2019); Ahlrichs et al., 2021. AFS: Agricola Fault System;*
 118 *EHT: Eastholstein Trough; EHMB: Eastholstein-Mecklenburg Block; PFZ: Prerow Fault Zone; STZ: Sorgenfrei-Tornquist Zone;*
 119 *TTZ: Teisseyre-Tornquist Zone; WF: Wiek Fault; WFZ: Werre Fault Zone; WPFS: Western Pomeranian Fault System.*

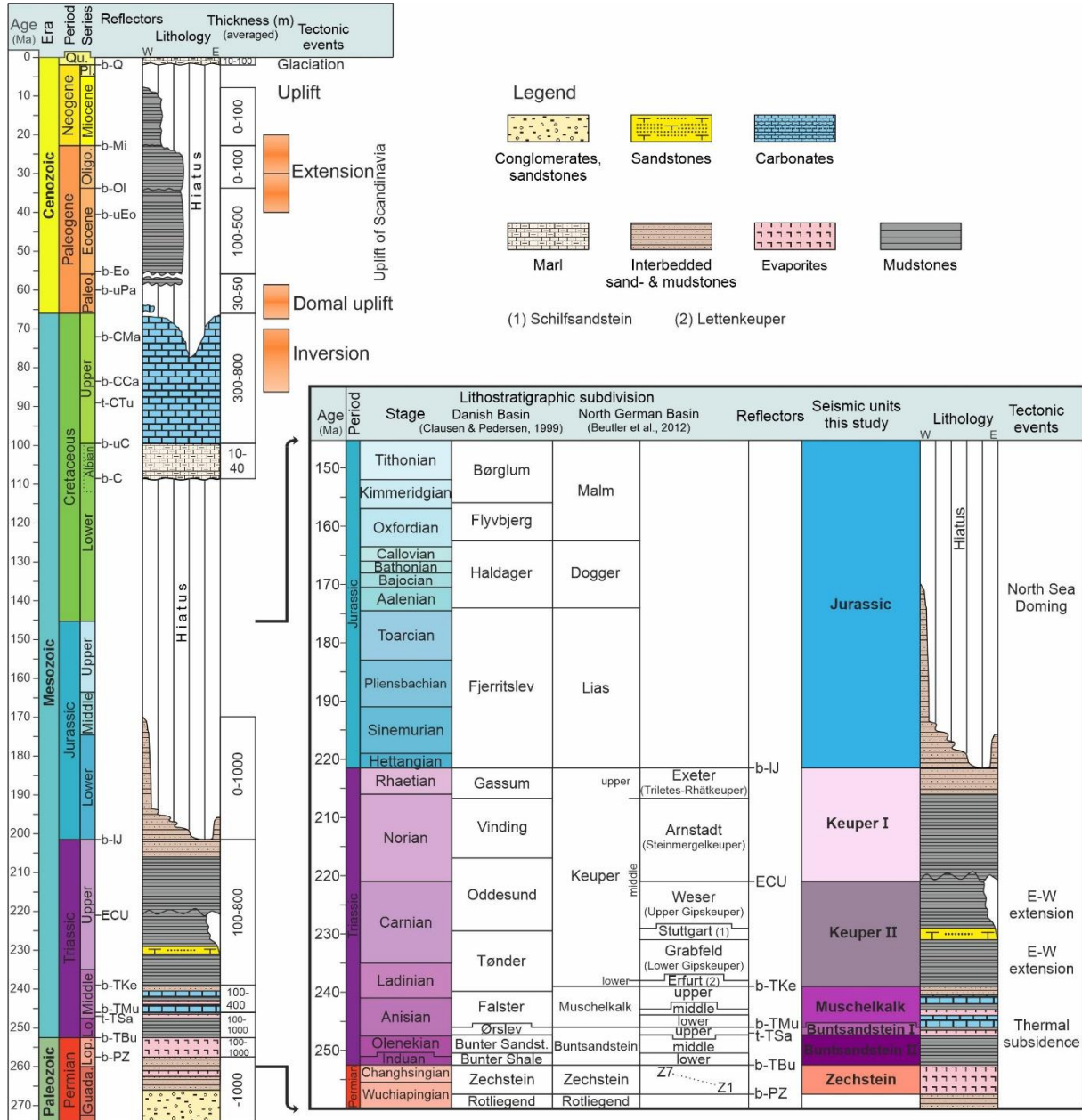
120 2. Geological Setting

121 The study area is located at the northern margin of the North German Basin (NGB) and extends from
 122 the Bay of Kiel in the west to the Bay of Mecklenburg and Rügen Island in the east (Fig. 1). The crust
 123 below the Baltic sector of the North German Basin consist of an assemblage of Caledonian and
 124 Variscan consolidated terranes and its transition to the Precambrian East European Craton (Fig. 1)
 125 (e.g. Guterch et al., 2010). This transition zone is termed the Trans-European Suture Zone and
 126 extends from the Caledonian Deformation Front in the north to the Elbe Lineament in the south (Fig.
 127 1) (Berthelsen, 1992; Guterch et al., 2010). The Ringkøbing-Fyn High, Møn High and Arkona High are a
 128 WNW-ESE trending series of basement highs (sensu Peacock & Banks, 2020), which separate the NGB
 129 and the Norwegian-Danish Basin (Fig. 1). In the western part of the study area, the NNE-SSW
 130 trending Mesozoic-Cenozoic Glückstadt Graben formed a NGB depocenter with up to 11 km of post-
 131 Permian sediment thickness strongly influenced by salt tectonics (e.g. Maystrenko et al., 2005a) (Fig.
 132 1). The Eastholstein Trough (EHT) marks the eastern part of the Glückstadt Graben and partly extends
 133 into the western Bay of Kiel. The central and eastern Bay of Kiel together with the Bay of
 134 Mecklenburg form the peripheral region between the Glückstadt Graben and the northeastern basin
 135 margin (Eastholstein-Mecklenburg Block (EHMB)), where the sedimentary infill of the basin amounts
 136 to 2 – 4 km (Fig. 1) (Maystrenko et al., 2005b). The eastern part of the study area is characterized by

137 the Western Pomeranian Fault System, a series of NW-SE to NNW-SSE striking faults often bordering
138 Y-shaped grabens (e.g. Werre Fault Zone, Prerow Fault Zone, Agricola Fault System, see Fig. 1)
139 (Krauss & Mayer, 2004).

140 Figure 2 briefly summarizes the development of the NGB showing the main tectonic events together
141 with the dominant lithology. In the late Carboniferous-early Permian, basin formation began with
142 wrench faulting, volcanism and lithospheric thinning followed by thermal subsidence (Ziegler,
143 1990b). During the late Permian, repeated restricted seawater influx under arid conditions led to
144 extensive evaporation and the deposition of the layered Zechstein evaporite succession within the
145 basin (Fig. 2) (Peryt et al., 2010; Strohmenger et al., 1996). Thermal subsidence lasted until the
146 Middle Triassic throughout the deposition of the Buntsandstein and Muschelkalk successions (Fig. 2)
147 (Van Wees et al., 2000). Locally, subsidence was enhanced by extension forming a narrow graben in
148 the central Glückstadt Graben during the Early and Middle Triassic (Brink et al., 1992).

149 An eustatic sea-level drop established terrestrial conditions in the Late Triassic during deposition of
150 the Keuper units (Nöldecke & Schwab, 1976). During the Late Triassic, E-W directed extension
151 widened the Glückstadt Graben and caused intensive salt movement including reactive diapirism
152 (Brink et al., 1992; Maystrenko et al., 2005b). Contemporaneously, the Zechstein salt started moving
153 in the other parts of the study area (Hansen et al., 2005; Hansen et al., 2007; Hübscher et al., 2010).
154 In the eastern part of the study area, Late Triassic extensional and dextral transtensional movements
155 caused the development of the Western Pomeranian Fault System (WPFS) by reactivation of
156 preexisting NW-SE oriented Paleozoic faults (Krauss & Mayer, 2004; Seidel et al., 2018).
157 Contemporaneously to the faulting in the WPFS, salt movement started in the Bay of Mecklenburg
158 (Ahlrichs et al., 2020). A major erosional unconformity, termed the Early Cimmerian Unconformity,
159 characterizes the Keuper succession in the study area (Beutler & Schüler, 1978). The unconformity is
160 especially prominent around Rügen Island, where in some areas the entire lower Keuper deposits are
161 missing (Beutler & Schüler, 1978). From Middle Jurassic times until the Albian, the North Sea Doming
162 event caused uplift and a phase of non-deposition during which widespread erosion removed much
163 of the Jurassic and partly Upper Triassic deposits in the study area (Fig. 2) (Ziegler, 1990b; Underhill &
164 Partington, 1993; Japsen et al., 2007; Hübscher et al., 2010). Jurassic deposits are almost exclusively
165 preserved in peripheral sinks of salt structures and are mostly of Early Jurassic age (Hoth et al., 1993;
166 Baldschuhn et al., 2001; Hansen et al., 2005; Zöllner et al., 2008; Hübscher et al., 2010). Assuming a
167 locally similar degree of erosion, the correlation of thicker remnants of Jurassic deposits with the
168 peripheral sinks could suggest ongoing salt movement during the Early Jurassic (Hansen et al., 2005;
169 Ahlrichs et al., 2020). Rising sea-levels led to resumed sedimentation in the Albian (Fig. 2). The
170 Cenomanian to Turonian succession was deposited in a period of relative tectonic quiescence
171 (Vejbaek et al., 2010). In the late Turonian to Santonian, a major plate reorganization and the onset
172 of the Africa-Iberia-Europe convergence subjected the study area to compressional stress leading to
173 inversion at the northern NGB margin (Fig. 2) (Kley & Voigt, 2008). Resulting horizontal shortening
174 caused uplift, erosion and fault reactivation and contemporaneous minor salt movement (Hübscher
175 et al., 2010; Al Hseinat & Hübscher, 2017; Ahlrichs et al., 2020). Following a phase of tectonic
176 quiescence, salt movement restarted during the late Eocene to Oligocene in the Glückstadt Graben
177 and likely also in the rest of the study area (Ahlrichs et al., 2021). In Miocene times, regional uplift led
178 to erosion of much of the Miocene, Oligocene and partly upper Eocene deposits (Hinsch, 1987;
179 Rasmussen, 2009; Japsen et al., 2015). Quaternary glaciation eroded further Neogene and Paleogene



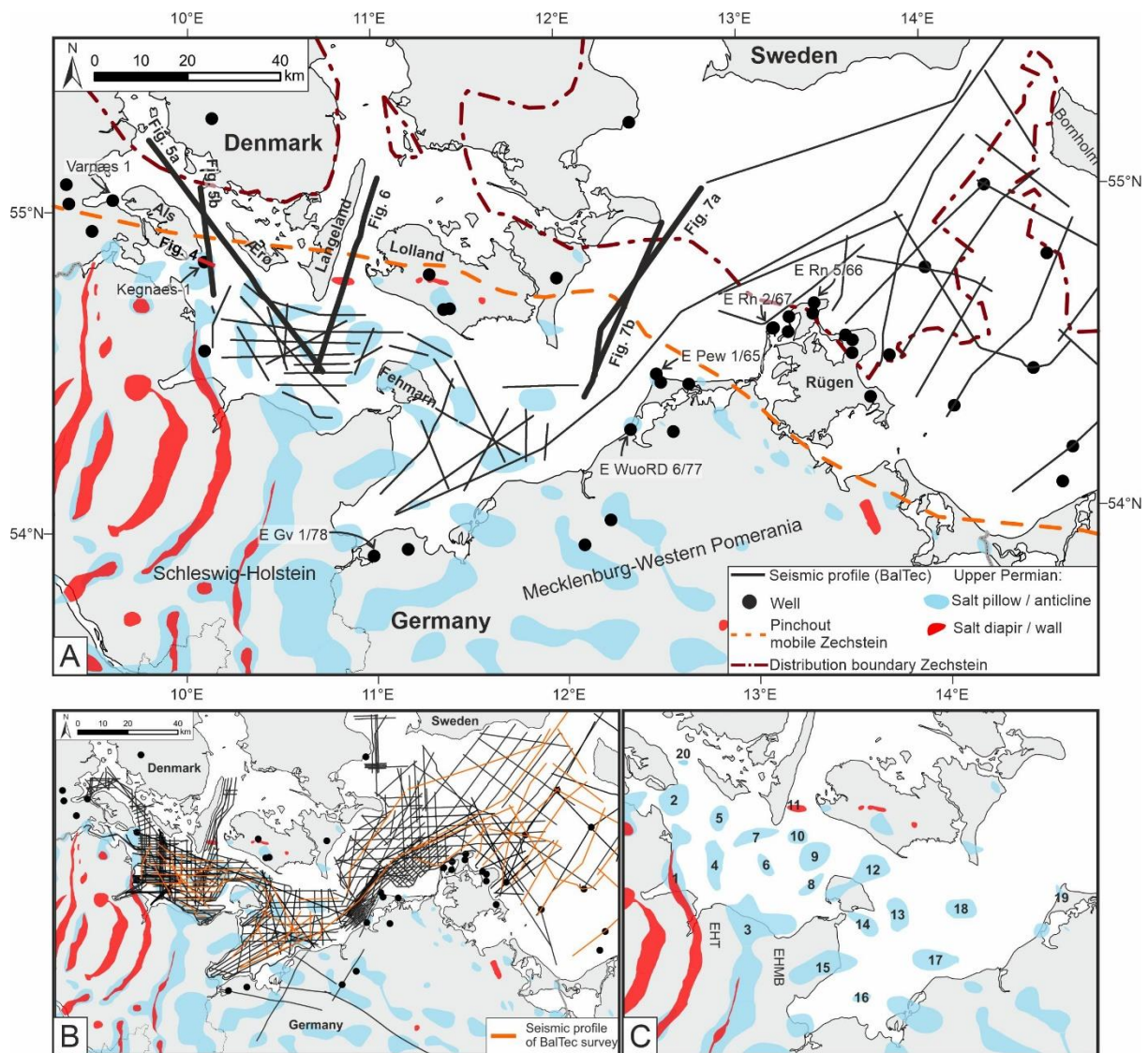
181
 182 Figure 2: Lithostratigraphic chart of the North German Basin showing dominant lithology, main tectonic events, average
 183 thickness and lithostratigraphic subdivision of the Triassic and Jurassic (Compiled from Clausen & Pedersen, 1999; Kossow &
 184 Krawczyk, 2002; Bachmann et al., 2008; Beutler et al., 2012; STD 2016; Ahlrichs et al., 2021). Reflectors modified after
 185 Ahlrichs et al. (2020). Reflectors: b-Q: base Quaternary Unconformity; b-Mi: base Miocene; b-Ol: base Oligocene; b-uEo:
 186 base upper Eocene; b-Eo: base Eocene; b-uPa: base upper Paleocene; b-CMa: base Upper Cretaceous Maastrichtian; b-CCa:
 187 base Upper Cretaceous Campanian; b-CTu: top Upper Cretaceous Turonian; b-uC: base Upper Cretaceous; b-C: base
 188 Cretaceous; b-IJ: base Lower Jurassic; ECU: Early Cimmerian Unconformity; b-TKe: base Triassic Keuper; b-TMu: base Triassic
 189 Muschelkalk; t-TSa: top Triassic Salinarröt; b-TBu: base Triassic Buntsandstein; b-PZ: base Permian Zechstein. Other
 190 abbreviations: Bunter Sandst.: Bunter Sandstone; Guada.: Guadalupian; Lo.: Lower; Lop.: Lopingian; Oligo.: Oligocene; Paleo.:
 191 Paleocene; PL.: Pleistocene; Qu.: Quaternary.

192 3. Database & Methods

193 3.1 Seismic database

194 The seismic database consists of high-resolution 2D seismic reflection data with a total profile length
 195 of more than 10,000 km acquired during multiple surveys (Fig. 3). These are seismic profiles of the
 196 BaltSeis and NeoBaltic projects (Hübscher et al., 2004, see Al Hseinat & Hübscher, 2017 for a detailed
 197 description), reprocessed profiles of the Petrobaltic database (Rempel, 1992; Schlüter et al., 1997),

198 profiles of the DEKORP-BASIN'96 survey (DEKORP-BASIN Research Group, 1999) and four industry
 199 profiles. The more local surveys were connected by the BalTec data (Hübscher et al., 2016), a
 200 regional network of high-resolution 2D seismic data imaging the subsurface continuously from the
 201 Zechstein salt base up to the seafloor (see Ahlrichs et al., 2020 for a more detailed description).

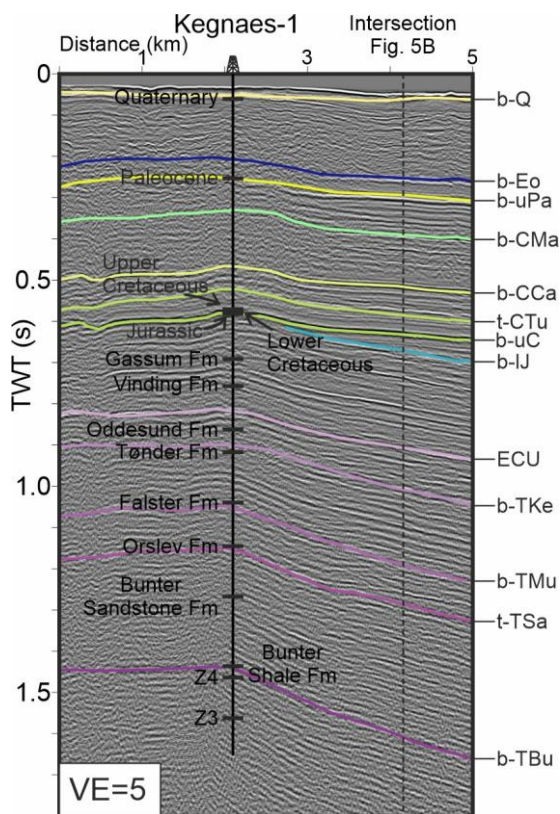


202
 203 *Figure 3: Seismic and well database (modified after Ahlrichs et al., 2021). A: Seismic profiles of the BalTec survey and*
 204 *locations of presented profiles together with wells in the study area. Key wells for the stratigraphic correlations are labelled.*
 205 *Distribution boundary of the Zechstein unit and pinch-out of mobile Zechstein units (low halite content does not allow salt*
 206 *movement) simplified after Katzung, 2004; Peryt et al., 2010; Seidel, 2019 B: Complete database with all available seismic*
 207 *profiles and wells used for mapping. C: Names of salt structures (after Vejbæk, 1997; Reinhold et al., 2008): 1: Waabs; 2:*
 208 *Bredgrund; 3: Plön; 4: Kieler Bucht; 5: Schleimünde; 6: Langeland Süd; 7: Langeland; 8: Flüggensand; 9: Vinsgrav; 10:*
 209 *Langeland Ost; 11: Kegnaes; 12: Fehmarn; 13: Staberhuk Ost; 14: Fehmarnsund Ost; 15: Cismar; 16: Boltenhagen Nord; 17:*
 210 *Trollegrund Nord; 18: Neobaltic; 19: Prerow; 20: Als Øst (discovered in this study).*

211 3.2 Stratigraphy

212 Stratigraphic interpretation is based upon the stratigraphic framework described by previous studies
 213 carried out within the *StrucFlow* project (Ahlrichs et al., 2020; Ahlrichs et al., 2021). Within this
 214 framework, 18 seismic horizons were identified: *base Quaternary Unconformity, base Miocene, base*
 215 *Oligocene, base upper Eocene, base Eocene, base upper Paleocene, base Maastrichtian, base*
 216 *Campanian, top Turonian, base Upper Cretaceous, base Cretaceous, base lower Jurassic, Early*
 217 *Cimmerian Unconformity, base Keuper, base Muschelkalk, top Salinarröt, base Buntsandstein, base*
 218 *Zechstein* (Fig. 2). In this study, we mostly focus on the Permian to Jurassic horizons. The calibration

219 of the seismic data with well information from deep research and hydrocarbon exploration wells was
 220 set up for the Bay of Mecklenburg and the area west of Rügen Island (Nielsen & Japsen, 1991; Hoth
 221 et al., 1993; Schlüter et al., 1997. Ahrichs et al. (2020) presented the most recent and comprehensive
 222 description and seismic-well-ties for wells located in the eastern part of the study area. From there,
 223 we traced the horizons across the study area using all available seismic data (Fig. 3). Additional
 224 control on the well-to-seismic tie was provided by the Kegnaes-1 well in the Bay of Kiel (Fig. 4) and
 225 additional Danish wells west of the Island of Als (Fig. 3) (Nielsen & Japsen, 1991). Furthermore, we
 226 linked the stratigraphic interpretation to previous onshore and offshore studies in the area
 227 (Michelsen, 1978; Clausen & Pedersen, 1999; Baldschuhn et al., 2001; Hansen et al., 2005;
 228 Maystrenko et al., 2005a, 2005b; Hansen et al., 2007; Zöllner et al., 2008; Hübscher et al., 2010; Al
 229 Hseinat et al., 2016; Deutschmann et al., 2018).



230
 231 *Figure 4: Well-to-seismic tie for the Kegnaes-1 well. Markers show the base of the units (Nielsen & Japsen, 1991). For*
 232 *location, see Fig. 3. See Fig. 2 for reflector abbreviations and juxtaposition of German and Danish lithostratigraphic units.*
 233 *Fm: Formation; VE: vertical exaggeration.*

234 3.3 Mapping

235 The mapping procedure includes gridding using all available horizon picks for each horizon to create
 236 two-way traveltimes (TWT) structure maps by minimum curvature spline interpolation with a grid cell
 237 size of 300 x 300 m. Only faults, which could be traced across multiple seismic profiles have been
 238 included in the maps. For time-depth conversion, a precise velocity model covering the entire study
 239 area is necessary. This is a challenging aspect of future work as velocity information is sparsely
 240 distributed due to the lack of offshore wells and seismic depth data. To give an idea of the depth
 241 range imaged by the presented seismic profiles, the right profile axis shows an approximated depth
 242 calculated using a constant velocity of 3 km/s. This velocity represents an average velocity of the
 243 subsurface in the study area based on published velocity information (Schnabel et al., 2021, see their
 244 table 1). We estimated the thickness of each mapped unit by calculating isochron maps (vertical
 245 thickness in TWT) for the Zechstein, Buntsandstein, Muschelkalk, Keuper II, Keuper I and Jurassic
 246 seismic units (see Fig. 2 for age constraints). To calculate the Jurassic isochron map, we used the base

247 Upper Cretaceous time-structure map of Ahlrichs et al. (2021). Thickness was converted from TWT to
248 meter by using a constant velocity selected for each unit based on previous studies (Schlüter et al.,
249 1997; Hansen et al., 2007; Schnabel et al., 2021).

250 3.4 Identification of salt movement

251 We analyze seismic profiles and isochron maps to identify local and regional thickness variations in
252 the Triassic and Jurassic units. Regional and local thickness variations are interpreted as an
253 expression of differential sedimentation and erosion caused by vertical tectonic movements,
254 differential compaction and sedimentation processes (Bertram & Milton, 1989). During synkinematic
255 sedimentation, the timing of the growth of a salt structure can be deduced from the surrounding
256 sediments by analyzing the geometric relationship between overburden strata and the salt structure
257 (e.g. Jackson & Hudec, 2017). Over geological time scales, salt can flow like a viscous fluid if the salt
258 body experiences differential loading by e.g. a varying gravitational load (e.g. by differential
259 sedimentation) or displacement loading (e.g. by extension or shortening) (Jackson & Hudec, 2017).
260 When salt flows from the surrounding area into the salt structure, the top of salt subsides in the area
261 of withdrawal, which creates additional accommodation space for more sediments. These processes
262 lead to increased thickness of the synkinematic unit if compared to adjacent areas without salt
263 movement (e.g. Jackson & Hudec, 2017). Likewise, the accumulation of salt decreases
264 accommodation space resulting in a thinner synkinematic unit above the salt structure. When the
265 regional sedimentation rate exceeds the rate of rise of the salt structure, the locally thickened
266 synkinematic strata in the peripheral sink (sensu Jackson & Hudec, 2017) is characterized by
267 converging and diverging layering (Sørensen, 1986). In the case of a regional sedimentation rate
268 smaller than the rise rate of the salt, angular unconformities between the layering of the peripheral
269 sink and the prekinematic overburden develop (Sørensen, 1986). Therefore, we interpret local
270 thickness variations across salt structures, characterized by thinning of the overburden towards the
271 crest and thickening of the overburden above the flanks of a salt structure (peripheral sink) as
272 evidence for syndepositional salt movement and salt structure growth. This includes a converging
273 and diverging reflector pattern, respectively. Accordingly, locally uniform thickness across salt
274 structures indicates the absence of salt movement.

275 4.Observations

276 We use key seismic profiles, time-structure and isochron maps of the Zechstein, Triassic and Jurassic
277 units to analyze the basin configuration, regional depositional patterns and local thickness variations
278 in order to identify active phases of salt movement during the Triassic-Jurassic.

279 4.1 Northwestern basin configuration

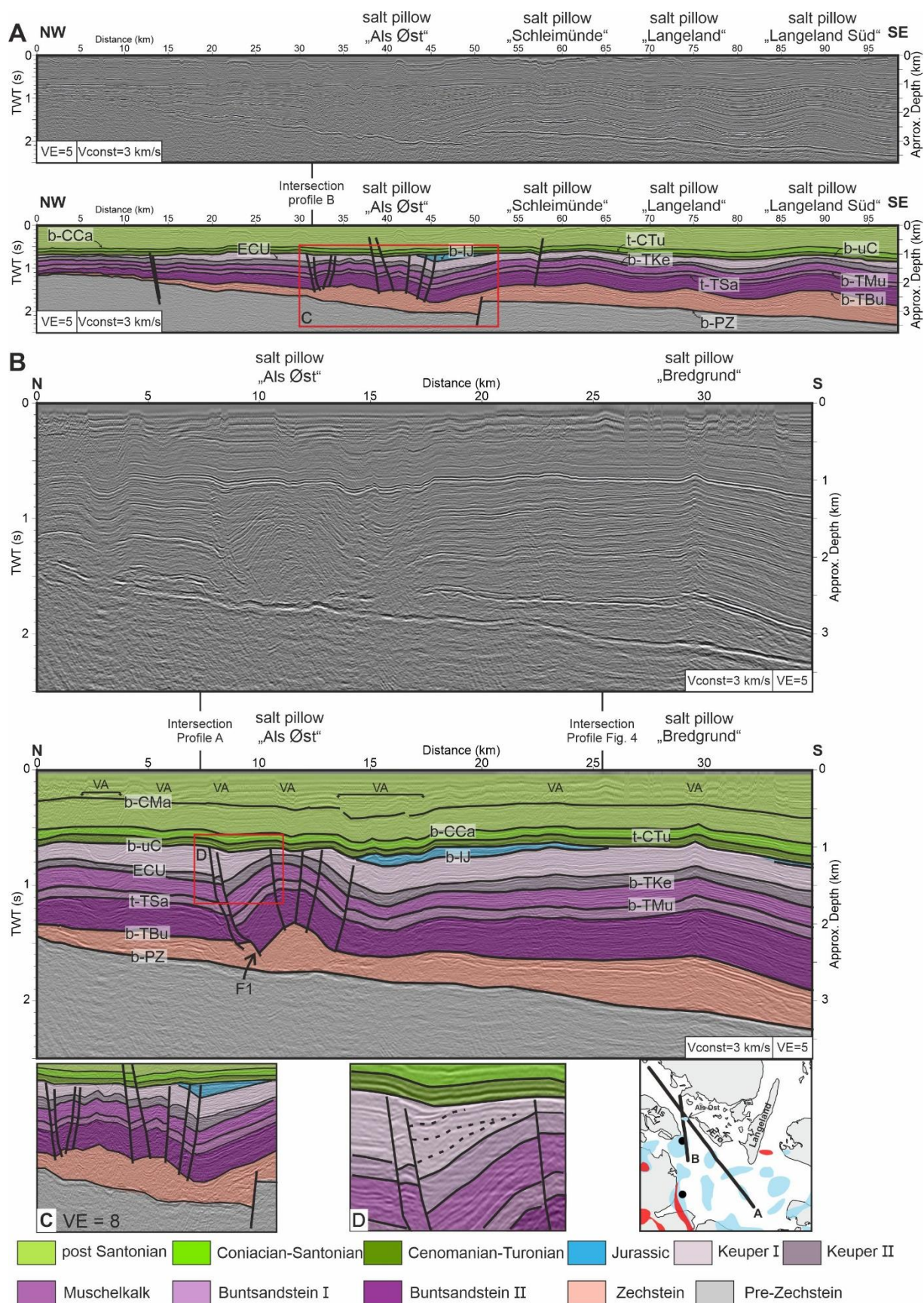
280 In the northwestern part of the study area, two profiles, which run from the basin margin
281 southwards into the Bay of Kiel, image numerous salt pillows (Fig. 5) (Vejbæk, 1997; Reinhold et al.,
282 2008). Faults pierce the base Zechstein at the basin margin (Fig. 5a, profile km 13). South of the
283 island of Ærø (Fig. 3), a prominent fault offsets the base Zechstein by ca. 300 ms TWT (Fig. 5a, profile
284 km 50). Between the islands of Als and Ærø, the profiles show a previously undescribed salt
285 structure, here named “Als Øst”, which is characterized by numerous faults in the Triassic-Jurassic
286 overburden (Fig. 5a and b). Thickness of the Buntsandstein and Muschelkalk units gradually increases
287 towards the south, and basin center, without any distinct local thickness variations and thus, no signs
288 for active salt movement (Fig. 5a and b).

289 The Keuper II unit is thin but uniform in thickness close to the basin margin in the northern part of
290 the profiles (Fig. 5). At the SE flank of the Als Øst salt pillow, this unit is characterized by increased
291 thickness, which indicates the onset of salt movement (Fig. 5a). Towards the southeast, the ECU
292 reflector erosionally truncates the Keuper II unit (Fig. 5a, profile km 50-55). Across the salt pillows

293 “Schleimünde” and “Langeland”, the Keuper II unit shows varying thickness by thinning towards the
294 crest of the structures indicating the initiation of salt structure growth during deposition of the
295 Keuper II (Fig. 5a). In the hangingwall of the listric fault north of the Als Øst salt pillow (F1 in Fig. 5b),
296 the Keuper II unit shows thickness variations. Additionally, the Keuper II unit has increased thickness
297 at the southern flank of the structure and slightly thins towards the crest of the Als Øst salt pillow,
298 which would suggest salt movement (Fig. 5b).

299 Throughout most of the profile, the Keuper I unit is capped at the top by the Mid Jurassic
300 Unconformity, expressed by the b-uC reflector (Fig. 5). At the northern flank of the Als Øst salt pillow,
301 the reflection pattern of the Keuper I unit is divergent towards the listric fault labelled with F1 in Fig.
302 5b (close up in Fig. 5c, note divergence between dashed lines and onlap). This suggests
303 syndepositional faulting and salt movement during the deposition of the Keuper I unit. Jurassic
304 deposits are only preserved in the peripheral sinks at the southern flank of the Als Øst salt pillow (Fig.
305 5).

306



307

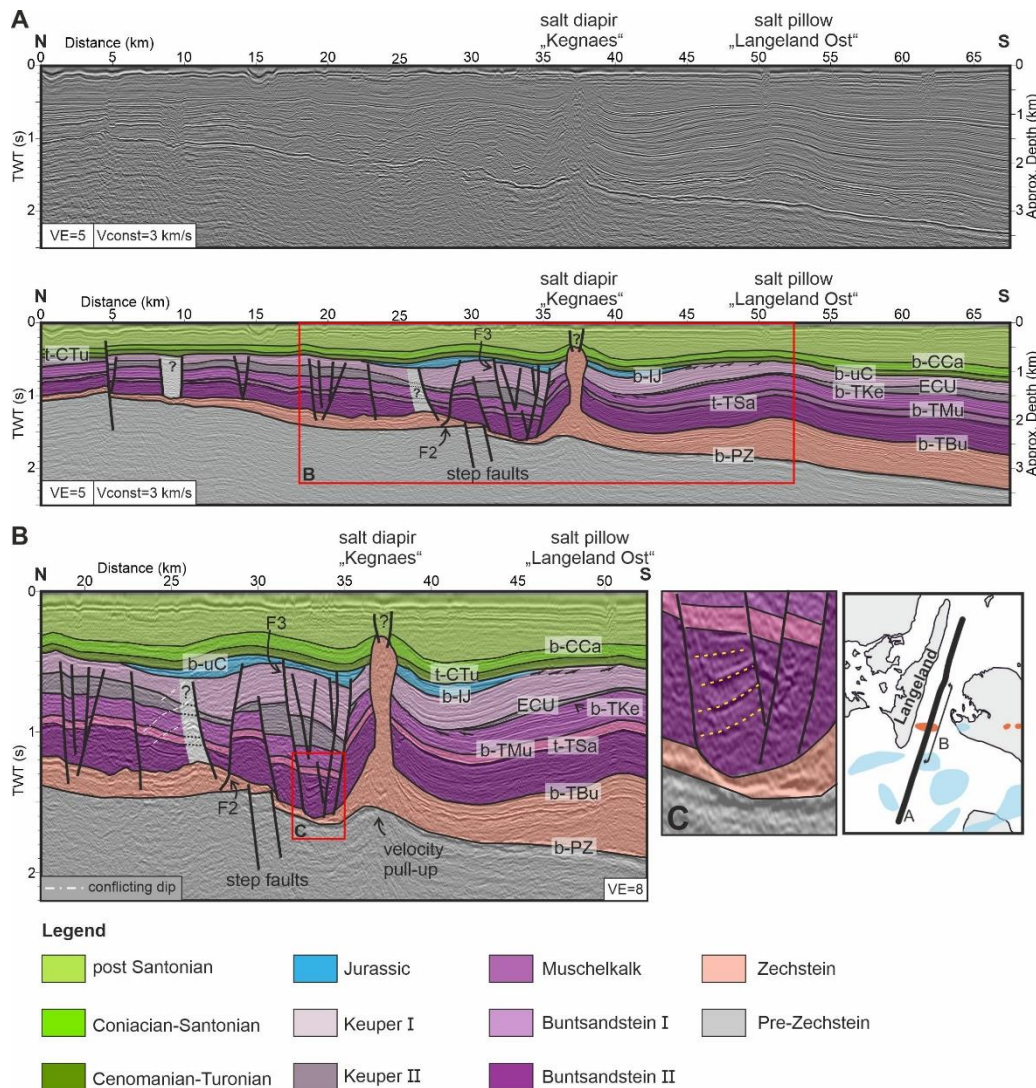
308

309

310

311

Figure 5: Time-migrated profiles A and B, located at the northwestern basin margin (see Fig. 3). An approximated depth is shown at the right axis of the profile (calculated using a constant velocity of 3 km/s). C: Enlargement of the Als Øst salt pillow. D: Enlargement of the Keuper I at the northern flank of the Als Øst salt pillow, note the divergent reflector pattern denoted by the dashed lines. VA: velocity artefact; VE: vertical exaggeration.



312
 313 *Figure 6: Time-migrated profile crossing the northern basin margin (see Fig. 3). An approximated depth is shown at the right*
 314 *axis of the profile (calculated using a constant velocity of 3 km/s). Stratigraphy in the light grey areas marked with “?” (ca.*
 315 *profile km 58 and 25) unknown due to highly disturbed reflection pattern. Exact extend of the roof and cover of the diapir*
 316 *unsure. Salt structures are marked on top of the section. Reflectors labeled as in Fig. 2. B: Enlargement as shown in A (with*
 317 *higher vertical exaggeration). Note the erosional termination of the Keuper II unit at the flanks of the diapir. C: Enlargement*
 318 *of B showing divergent reflections within the Buntsandstein north of the Kegnaes Diapir. VE: Vertical exaggeration.*

319 4.2 Northern basin configuration and the Kegnaes Diapir

320 In the central part of the study area, a N-S striking profile runs from the basin margin into the Bay of
 321 Kiel imaging the salt diapir “Kegnaes” (Fig. 6) (Vejbæk, 1997). The width of the diapir is ca. 1 km at its
 322 top and 3 km at its root. The narrow stem suggests that the diapir was mildly squeezed. In the
 323 southern part of the profile, an approx. 1.5 km wide zone with highly disturbed reflection pattern
 324 and uncertain stratigraphy is visible (Fig. 6a, profile km 8). North of the Kegnaes Diapir (KD), the
 325 Triassic overburden above the strongly reduced Zechstein salt shows increased thickness and is
 326 intensely faulted (Fig. 6a and b). Beneath, two basement step faults pierce the base Zechstein
 327 without reaching further into the suprasalt overburden.

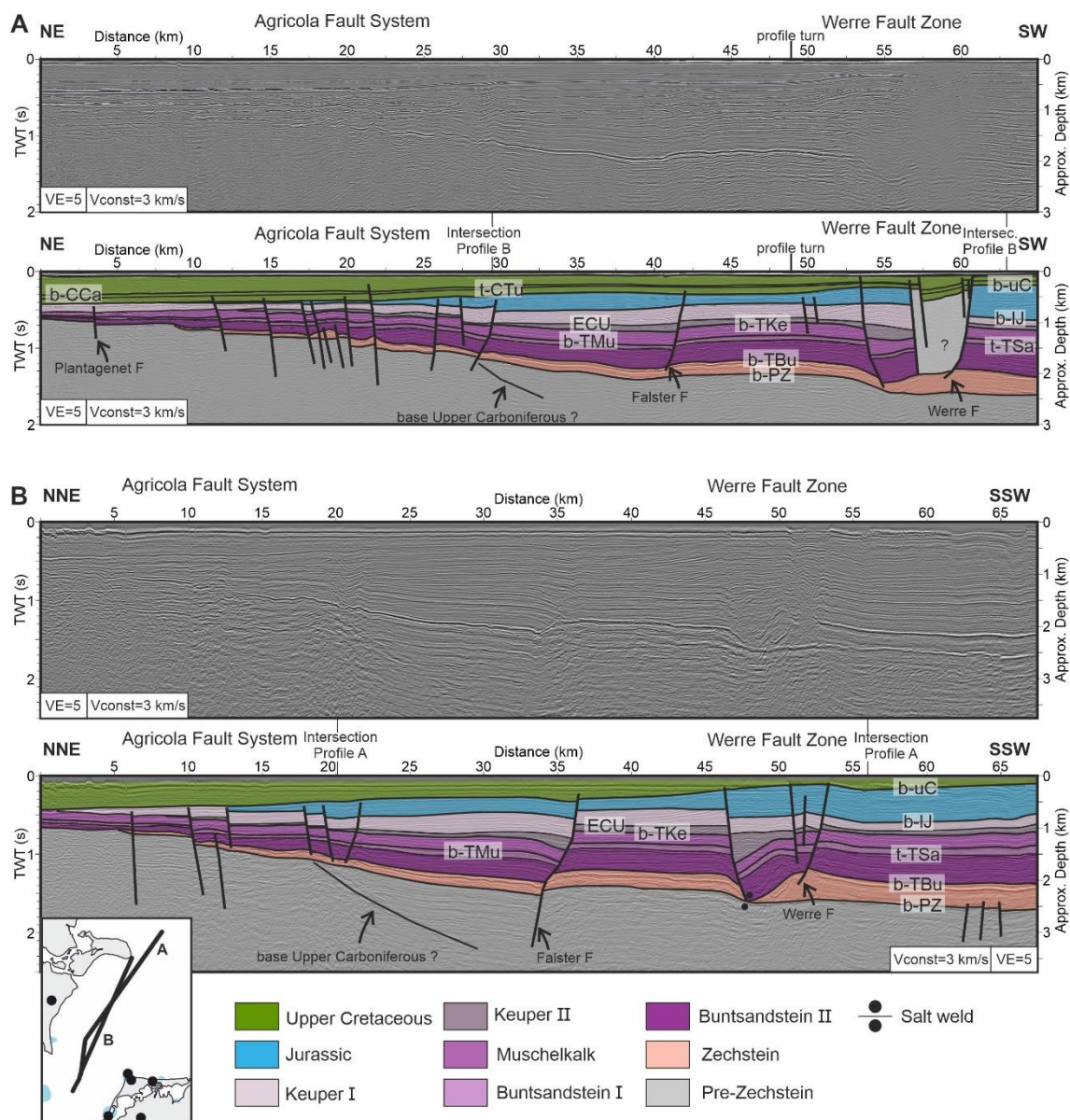
328 Overall, the Buntsandstein unit shows a general trend of gradually increasing thickness towards the
 329 south-directed basin center. The exception to this trend is a zone, where the Buntsandstein locally
 330 thins towards the south until reaching the northward dipping fault F2 (Fig. 6a and b, profile km 23 -
 331 28). Noteworthy, this zone is located about a kilometer north and above the footwall of the
 332 basement step faults (Fig. 6a and b). Above the northern flank of the diapir, the Buntsandstein unit

333 within the hangingwall of the F3 labelled fault shows divergent reflectors towards the fault (Fig. 6c),
334 which indicate an early phase of faulting. Towards the diapir, the Buntsandstein slightly thins
335 suggesting salt movement coeval to the faulting (Fig. 6b-c). The Muschelkalk concordantly overlies
336 the Buntsandstein and shows relatively constant thickness across the profile (Fig. 6a). The Keuper II
337 unit has a relative uniform thickness in the northern part of the profile. Between profile km 23 – 28,
338 the Keuper II unit dips towards the south and gradually thins. In this area, multiple conflicting dips
339 cross the Keuper unit. These conflicting dips are probably caused by out of plane reflections
340 originating from the sides of the 2D profile (see e.g. Drummon et al., 2004). In the fault zone north of
341 the diapir, the Keuper II unit has increased thickness (Fig. 6b). This zone represents the primary
342 peripheral sink and indicates salt movement and normal faulting (Fig. 6b). At both flanks of the
343 diapir, the Keuper II terminates in a toplap against the ECU reflector. Salt movement and faulting
344 continued during deposition of the Keuper I indicated by the increased thickness within the faulted
345 zone and at the southern flank of the diapir (Fig. 6b). Right there, Jurassic deposits were preserved
346 from erosion. The Cenomanian – Turonian and Coniacian – Santonian units overly the Triassic-
347 Jurassic deposits without visible thickness variations. (Fig. 6a, b). At the flanks, these units are slightly
348 folded and terminate against the diapir. The Cretaceous directly above the crest of diapir is unclear
349 as the seismic image does not resolve the shallow strata in the uppermost part of the profile (Fig.
350 6b).

351 4.3 Northeastern basin configuration

352 In the northeastern part of the study area, two profiles image the basin margin and the pinch-out of
353 the Zechstein unit (Fig. 7). In the northeastern part of the profiles, multiple basement faults pierce
354 the southward dipping base Zechstein (Agricola Fault System, Fig. 7). The Falster Fault imaged by the
355 profile in Fig. 7a only pierces the Mesozoic overburden while in the profile located further east, the
356 fault reaches into the pre-Zechstein (Fig. 7b). In the southwestern part, faults of the Werre Fault
357 Zone (Werre FZ) only pierce the Mesozoic overburden (Fig. 7). The Buntsandstein and Muschelkalk
358 units gradually increase in thickness towards the basin center further south without local thickness
359 variations, and thus, no signs of syndepositional faulting.

360 The Keuper II unit in the hangingwall of the Falster Fault has increased thickness, which suggests
361 initial syndepositional faulting (Fig. 7). The northeastern border fault of the WFZ is a SW-dipping
362 slightly listric fault where the Keuper II unit shows increasing thickness towards the fault (Fig. 7b). In
363 between the WFZ and Agricola Fault System (Agricola FS), the thickness of the Keuper I unit is
364 approximately doubled, which suggests increased subsidence in this area (Fig. 7). Increased thickness
365 of the Keuper I unit in the hangingwall of the Falster Fault suggests ongoing normal faulting (Fig. 7b).
366 The Keuper I unit within the WFZ shows increased thickness compared to southwest of the Werre
367 Fault, however, the unit shows an almost horizontal position (Fig. 7b).



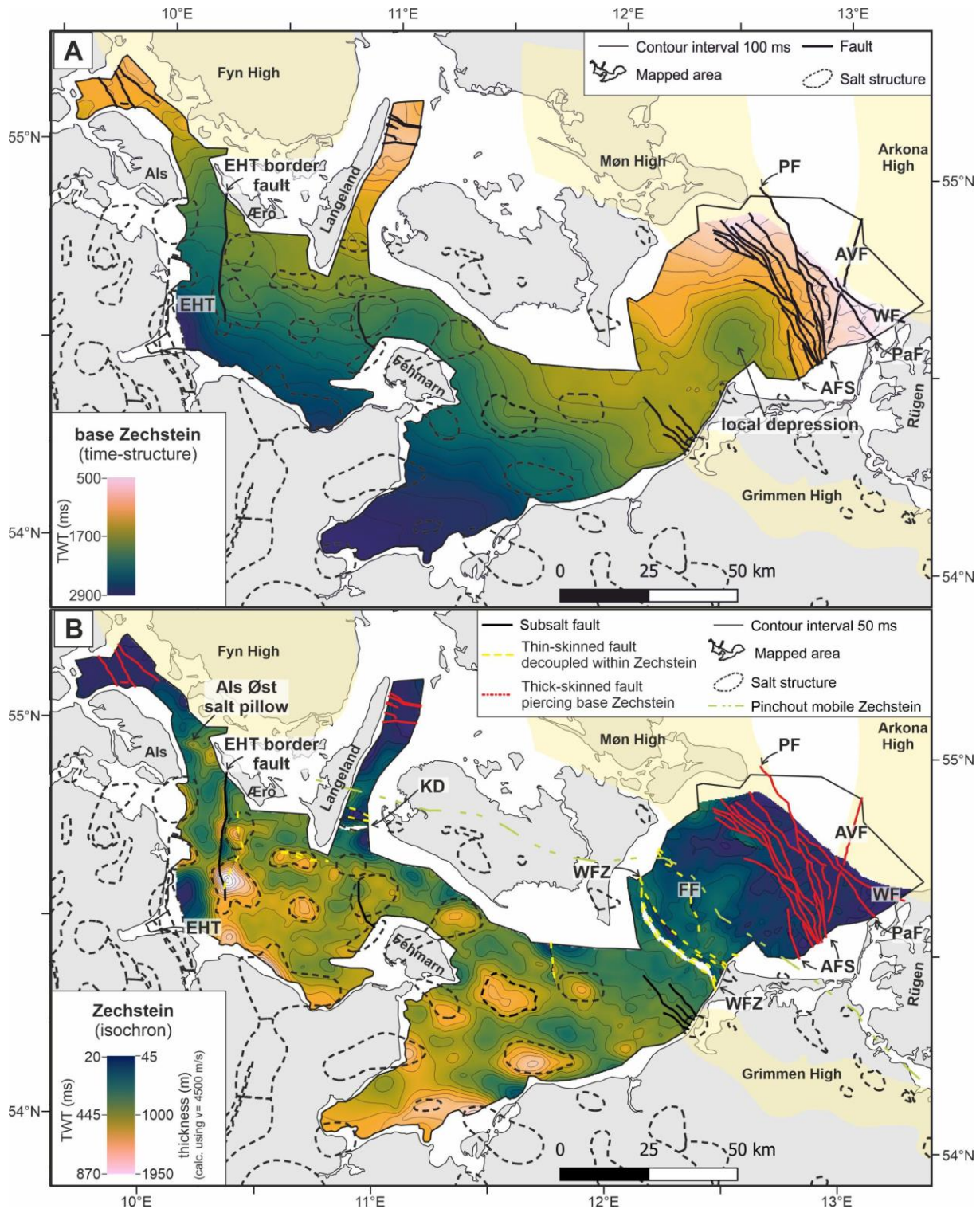
368

369 *Figure 7: Time-migrated profiles A (BGR16-221) and B imaging the northeastern basin margin. See Fig. 3 for location. Fault*
 370 *systems are marked at the top of the sections. An approximated depth is shown at the right axis of the profile (calculated*
 371 *using a constant velocity of 3 km/s). Note the profile turn and thus different profile orientation of A and B and resulting*
 372 *different appearance of structures, especially of the Werre Fault Zone. VE: vertical exaggeration. F: fault. Reflectors labeled*
 373 *as in Fig. 2. See Ahlrichs et al. (2020) for an additional profile imaging this area.*

374 4.4 Mapping of stratigraphic units

375 4.4.1 Zechstein

376 The base Zechstein shallows from 2900 ms TWT, representing the central part of the basin, towards
 377 its pinch-out at the northeastern basin margin at ca. 500 ms TWT (Fig. 8a). West of Rügen Island, the
 378 NE-SW trend is locally interrupted by an approx. 20 km wide depression (Fig. 8a). Across the basin
 379 margin, multiple faults pierce the base Zechstein (Fig. 8a, faults marked with AFS, PF, WF, PaF, AVF
 380 and faults near the islands of Langeland and Als). Additional faults with partly small offsets are visible
 381 northwest of the Grimmen High and northwest of Fehmarn Island. In the western Bay of Kiel, a
 382 prominent fault showing a large offset of the base Zechstein (as imaged by Fig. 5a) strikes N-S,
 383 parallel to the salt structures Schönberg-Kieler Bucht (Fig. 8a). This fault marks the eastern border of
 384 the EHT. Thickness of the Zechstein unit correlates well with the known locations of salt structures
 385 (Figs. 1 and 8b). Mapping reveals a new small salt pillow named “Als Øst” (Figs. 8b and Fig. 5).



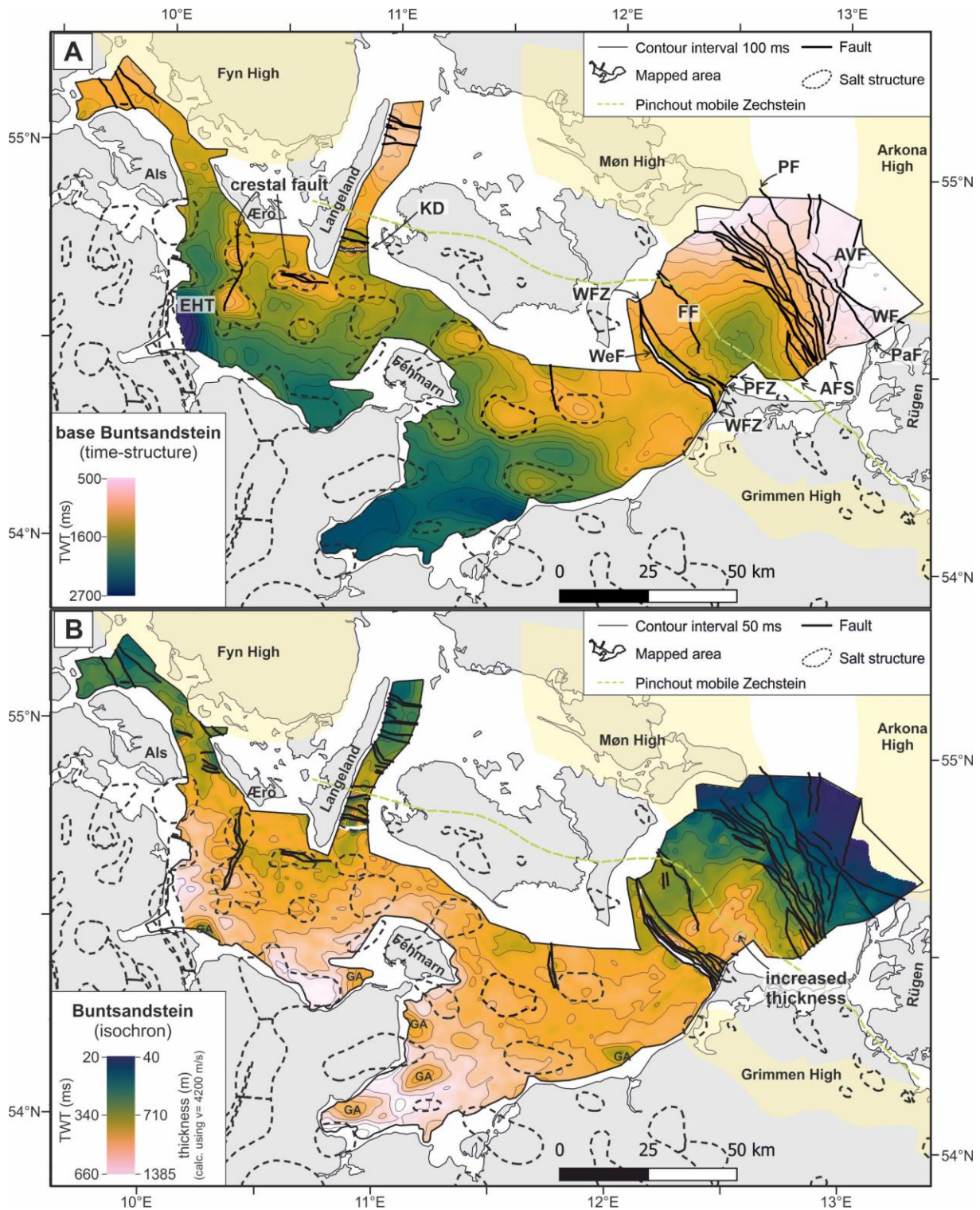
386

387 Figure 8: Zechstein. A: base Zechstein time-structure map in TWT. B: Zechstein isochron map in TWT. AFS: Agricola Fault
 388 System; AVF: Agricola-Svedala Fault; EHT: Eastholstein Trough; FF: Falster Fault; KD: Kegnaes Diapir; PaF: Parchim Fault; PF:
 389 Plantagenet Fault; WF: Wiek Fault; WFZ: Werre Fault Zone.

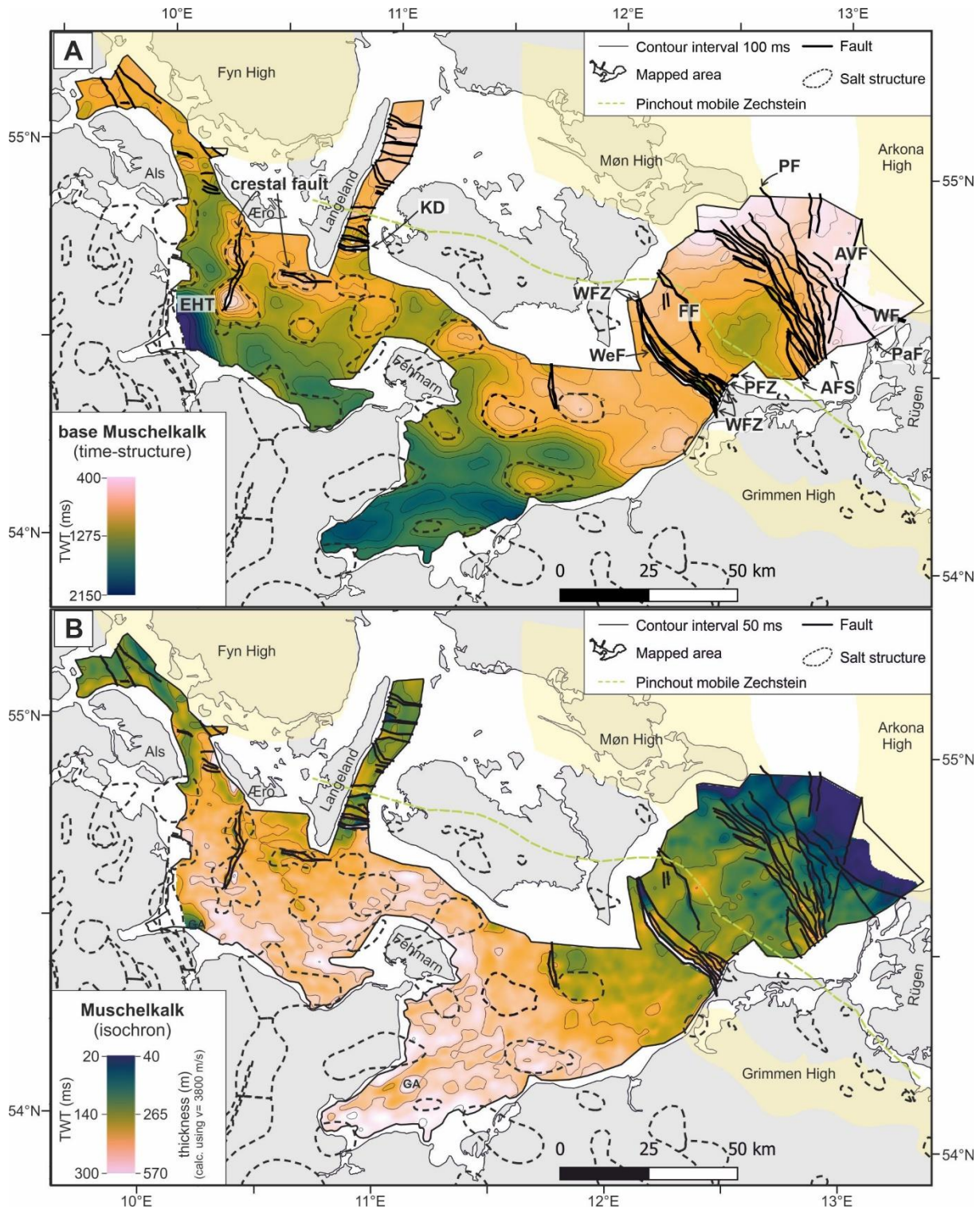
390 4.4.2 Buntsandstein and Muschelkalk

391 The base Buntsandstein and base Muschelkalk time-structure maps show the general N-S to NE-SW
 392 trend from the shallow margin towards the deeper basin locally modified by the presence of
 393 Zechstein salt structures (Figs. 9a and 10a). Thickness of the Buntsandstein and Muschelkalk units
 394 gradually increase towards the basin center due to the higher degree of subsidence away from the
 395 basin margins (Figs. 9b and 10b). Thickness variations are close to seismic resolution (ca. 50 ms TWT,

396 ca. 75 m, 3 km/s) and do not correlate with the salt structures Between the Werre FZ and Agricola FS,
 397 the isochron map of the Buntsandstein unit reveals a zone of locally increased thickness (Fig. 9b). In
 398 the Muschelkalk, this zone of increased thickness is not visible (Fig. 10b).



399
 400 *Figure 9: Buntsandstein. A: base Buntsandstein (top Zechstein) time-structure map in TWT. B: Buntsandstein isochron map in*
 401 *TWT. AFS: Agricola Fault System; AVF: Agricola-Svedala Fault; EHT: Eastholstein Trough; FF: Falster Fault; KD: Kegnaes*
 402 *Diapir; PaF: Parchim Fault; PF: Plantagenet Fault; PFZ: Prerow Fault Zone; WF: Wiek Fault; WeF: Werre Fault; WFZ: Werre*
 403 *Fault Zone. GA: Gridding artefact caused by either lack of seismic data in the area or velocity artefacts by e.g. shallow gas.*



404

405 *Figure 10: Muschelkalk. A: base Muschelkalk time-structure map in TWT. B: Muschelkalk isochron map in TWT. See Fig. 9 for*
 406 *abbreviations.*

407 **4.4.3 Keuper**

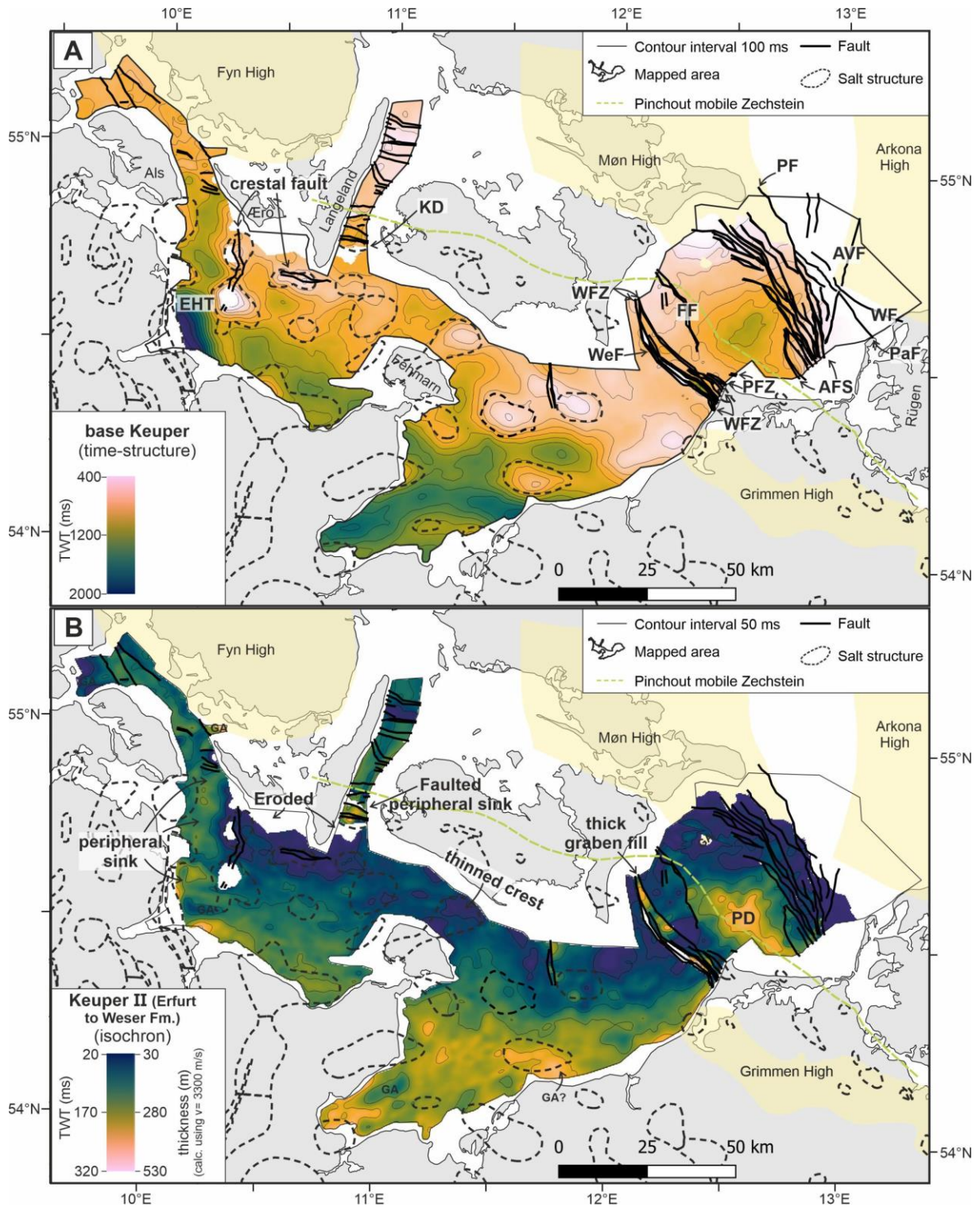
408 The base Keuper time-structure map shows a similar pattern as the base Muschelkalk (Fig. 11a). The
 409 isochron map of the Keuper II unit reveals the general thickening trend towards the south (Fig. 11b).
 410 At the northeastern basin margin, south of the Island of Æro and south of the KD, the Keuper II unit
 411 is eroded (Fig. 11a and b). Further modifications to the general thickness trend are visible between
 412 the Werre FZ and Agricola FS, where the thickness of the Keuper II is locally more than doubled (Fig.
 413 11b, PD: Prerow Depression). The graben within the Werre FZ shows increased infill with Keuper II

414 sediments (Fig. 11b). Furthermore, the Keuper II isochron map shows local thickness variations
415 across salt structures such as the thinned crest of the Fehmarn salt pillow and the development of
416 the northern peripheral sink of the KD, which is also intensely faulted (Fig. 11b). In the EHT, thickness
417 of the Keuper II is increased. In the Bay of Mecklenburg, the Keuper II isochron map shows a zone of
418 locally increased thickness at the southern border of the gridded area expanding across the crest of
419 the Trollegrund Nord salt pillow, which is unexpected in terms of salt movement. Due to the
420 connection to the edge of the mapped area, this zone of increased thickness possibly represents a
421 gridding artefact.

422 In many parts of the study area, the Keuper I is affected by erosion related to the Mid Jurassic
423 Doming. Thus, when interpreting thickness variations of the Keuper I, one needs to consider that in
424 areas where the Jurassic is missing, the top of the Keuper I unit is eroded too and the present
425 thickness represent the thickness preserved from erosion (Fig. 12b, white line and Fig. 13). Between
426 the Werre FZ and Agricola FS, thickness of the Keuper I is increased (Fig. 12b). Compared to the
427 Keuper II unit, the zone of increased thickness widened and the local depocenter shifted northwest
428 (compare area marked with PD in Fig. 12b and 11b). Northwest of the Grimmen High, the Keuper I is
429 thinned and the thickness trend shows a local E-W direction (Fig. 12b). Northeast of the salt pillow
430 "Trollegrund Nord" in the Bay of Mecklenburg, north of the KD and in the EHT, thickness of the
431 Keuper I is locally increased (Fig. 12b).

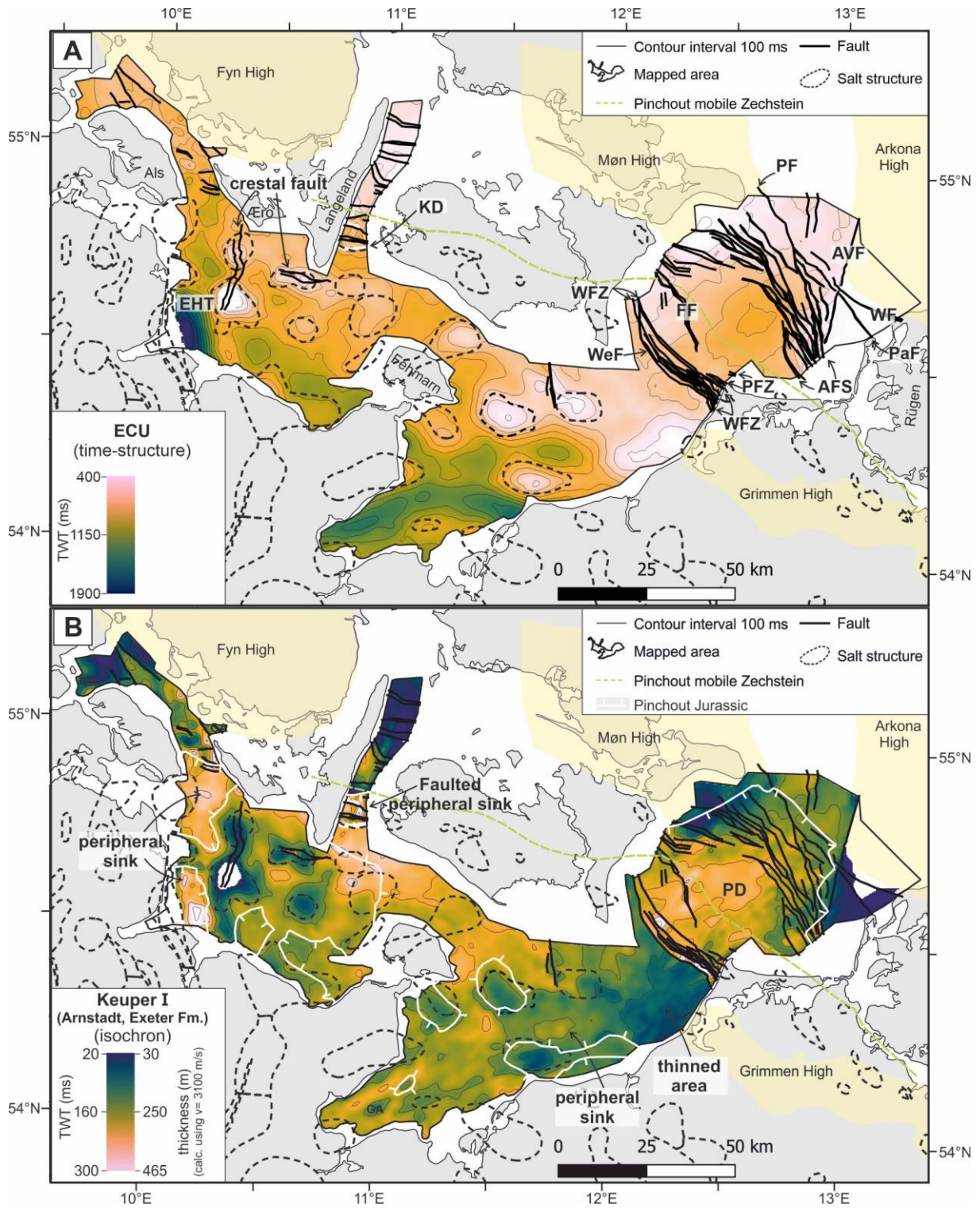
432 4.4.4 Jurassic

433 The base Jurassic time-structure map shows the strongly disrupted character of the unit (Fig. 13a).
434 Maximum thickness is visible in the Prerow Depression (Fig. 13b). Compared to the Keuper I unit, this
435 zone of increased thickness further widened and includes the area southwest of the Werre FZ. In the
436 Bay of Mecklenburg, the preserved Jurassic unit is thin and completely eroded above the crest of salt
437 structures (Fig. 13b). In the Bay of Kiel, almost the entire Jurassic unit is missing. Across the study
438 area, the Jurassic unit is thin or reduced above the crest of salt structures while thicker Jurassic
439 remnants are located above the flanks (Fig. 13b).



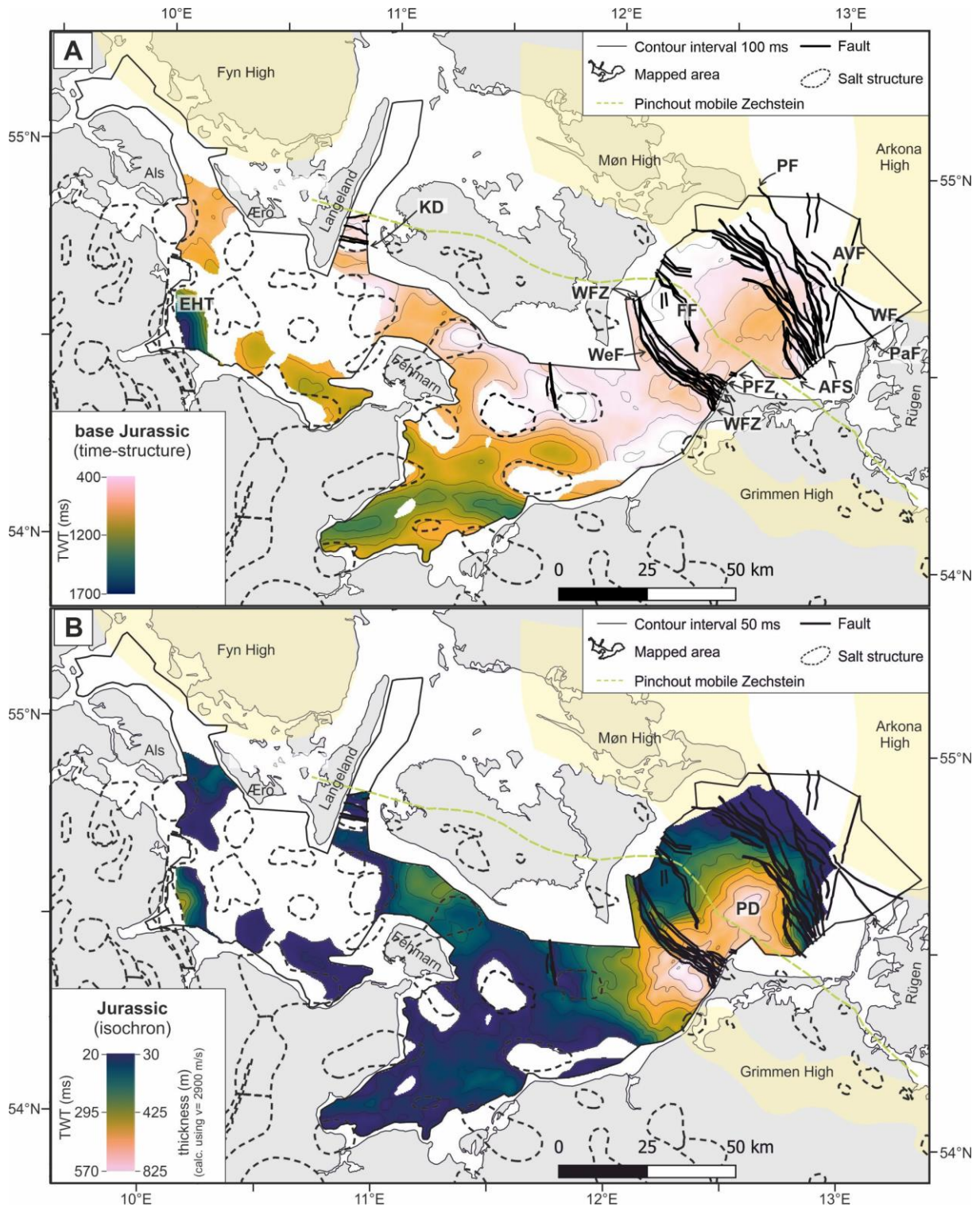
440

441 *Figure 11: Keuper II. A: base Keuper time-structure map in TWT. B: Keuper II isochron map in TWT. Note the absence of*
 442 *Keuper II deposits adjacent to the islands of Æro and Langeland and northwest of Rügen due to erosion causing the Early*
 443 *Cimmerian Unconformity (ECU). PD: Prerow Depression. See Fig. 9 for further abbreviations.*



444

445 Figure 12: Keuper I. A: Early Cimmerian Unconformity (ECU) time-structure map in TWT. B: Keuper I isochron map in TWT.
 446 White line shows area of preserved Jurassic deposits, hence, where the Keuper I was spared from Mid Jurassic erosion. PD:
 447 Prerow Depression; see Fig. 9 for further abbreviations.



448

449 *Figure 13: Jurassic. A: base Jurassic time-structure map in TWT. B: Jurassic isochron map in TWT. The entire Jurassic unit was*
 450 *affected by strong Mid Jurassic erosion and thus, mapped thickness only represent preserved remnants. PD: Prerow*
 451 *Depression; see Fig. 9 for further abbreviations.*

452 5. Interpretation and Discussion

453 In the following, we will interpret and discuss our observations in the context of the existing
 454 literature covering the timing of salt movement throughout the study area and faulting at the
 455 northeastern basin margin.

456 5.1 Comparison with previous work

457 The south to southwest dip of the base Zechstein, pinch-out of the Zechstein unit at the northeastern
458 basin margin and location of salt structures within the study area (Figs. 5 - 8) are in agreement with
459 the overall known basin configuration (Peryt et al., 2010). The trend of increasing thickness of the
460 Buntsandstein and Muschelkalk towards the south-directed basin center (Figs. 9 and 10) is in
461 accordance with previous studies and likewise explained by thermal subsidence from late Permian to
462 Middle Triassic times (Baldschuhn et al., 2001; Kossow & Krawczyk, 2002; Hansen et al., 2005; Zöllner
463 et al., 2008; Hübscher et al., 2010). Thereby, subsidence was highest in the basin center leading to
464 increased sedimentary infill with Buntsandstein and Muschelkalk deposits (Scheck & Bayer, 1999;
465 Van Wees et al., 2000). Local modifications of this trend could result from differential compaction,
466 sea level fluctuations and sedimentation processes, which might have caused e.g. the visible
467 thickness variations of the Buntsandstein in the central Bay of Mecklenburg or of the Muschelkalk
468 northwest of Fehmarn Island (Figs. 9 and 10) (Bertram & Milton, 1989).

469 The observed Late Triassic erosion causing the ECU (Figs. 11 and 12) is in accordance to previous
470 studies (Beutler & Schüler, 1978; Bachmann et al., 2010). Adding to the existing maps (e.g. subcrop
471 map of the ECU in Bachmann et al., 2010), we observe erosion of the entire lower and middle Keuper
472 unit underlying the ECU south of Æro island, west of Langeland and south of the KD (Fig. 11). Hence,
473 the area affected by Late Triassic erosion seems to stretch across the entire southern margin of the
474 Ringkøbing-Fyn, Møn and Arkona highs, which fits to the observations of Clausen and Pedersen
475 (1999) based on onshore seismic profiles and well data.

476 This study provides an update to the published fault pattern and differentiates between subsalt and
477 suprasalt faults (Figs. 8 and 9-13). Northwest of the Grimmen High, we identified subsalt faults solely
478 dissecting the PreZechstein, which likely form the offshore prolongation of faults visible in the TUNB
479 model onshore Mecklenburg-Western Pomerania (TUNB Working Group, 2021). A bit further
480 northeast, the Werre FZ marks a thin-skinned fault zone only affecting the Zechstein and suprasalt
481 overburden. These faults show the decoupling effect of the Zechstein salt and accordingly, thickness
482 of the Zechstein in this part of the basin and further south is sufficient to effectively decouple the
483 suprasalt cover from the basement (e.g. Stewart et al., 1996; Withjack & Callaway, 2000).
484 Furthermore, our mapping shows a prominent basement fault in the western Bay of Kiel, which we
485 interpret as the eastern border fault of the EHT (Fig. 5 and 8). The fault trace coincides with maps of
486 Vejrbæk (1997) and was imaged by Ahlrichs et al. (2021) (their Fig. 5). The salt structures “Kieler
487 Bucht” and “Schönberg” strike parallel to the fault and are located directly adjacent to it. The
488 development of these salt structures is likely controlled by the underlying basement fault decoupled
489 by the thick Zechstein salt (Stewart et al., 1996; Withjack & Callaway, 2000; Warren, 2008). This is in
490 agreement with many salt structures, which are underlain by basement faults in other parts of the
491 Glückstadt Graben (e.g. Baldschuhn et al., 2001; Maystrenko et al., 2005b).

492 5.2 Timing of salt movement

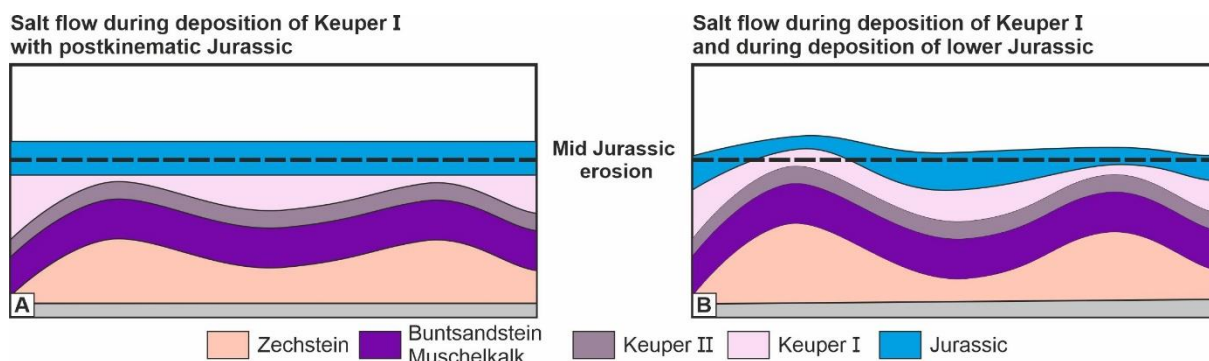
493 The triggering of salt movement in the Baltic sector of the North German Basin driven by extension
494 during the Late Triassic is well established (Clausen & Pedersen, 1999; Hansen et al., 2005; Hansen et
495 al., 2007; Zöllner et al., 2008; Hübscher et al., 2010; Al Hseinat et al., 2016). Using a single seismic
496 profile located in the Bay of Mecklenburg, Ahlrichs et al. (2020) established a refined stratigraphic
497 subdivision of the Triassic, which revealed initial salt movement during deposition of the Keuper II
498 unit. This study provides regional maps of the Buntsandstein, Muschelkalk, Keuper and Jurassic units

499 with the refined stratigraphic subdivision established by Ahlrichs et al. (2020) to analyze the spatial
500 character of salt movement in the Baltic sector of the North German Basin.

501 The Buntsandstein and Muschelkalk units do not show local thickness variations and thus, were
502 deposited prior to the development of the salt structures (Figs. 9 and 10). This prekinematic phase
503 during the Early and Middle Triassic in the eastern Glückstadt Graben and EHMB agrees with
504 previous onshore and offshore studies (Hansen et al., 2005; Maystrenko et al., 2005b; Zöllner et al.,
505 2008; Hübscher et al., 2010; Al Hseinat et al., 2016; Warsitzka et al., 2016). Notably, the increasing
506 thickness of the Buntsandstein and Muschelkalk units towards the basin center, which represents a
507 differential load acting on the Zechstein salt, did not trigger salt movement in the Baltic sector of the
508 North German Basin. A possible explanation would be that the gradually increasing thickness of the
509 Buntsandstein and Muschelkalk represents only subtle thickness variations for the scale of salt
510 structures. Thus, forces driving salt flow by the differential loading might not be sufficient to
511 overcome resisting forces of salt flow (like boundary friction and strength of the overburden) (Hudec
512 & Jackson, 2007; Warsitzka et al., 2013).

513 *5.2.1 Eastholstein Trough*

514 Local thickness variations of the Keuper II unit, indicate initial salt movement in the Eastholstein
515 Trough (EHT) (Fig. 11). This is in agreement with previous studies covering the Glückstadt Graben and
516 northwest Germany, where discrete pulses of extension and salt movement were observed in the
517 early Late Triassic during deposition of the Grabfeld and Weser formations (Frisch & Kockel, 1999;
518 Kockel, 2002; Maystrenko et al., 2005b; Al Hseinat et al., 2016). Salt movement continued during
519 deposition of the Keuper I unit in the EHT (Fig. 12), even though extension abated (Frisch & Kockel,
520 1999). We explain the ongoing salt structure growth by differential loading induced by the foregone
521 extensionally triggered salt flow (Kehle, 1988; Hudec & Jackson, 2007). Jurassic sediments were
522 strongly affected by erosion related to the Mid Jurassic Doming event. Thus, the present-day
523 thickness represents the thickness of the remnants preserved from erosion and cannot be used
524 directly to infer active salt flow. Preserved Jurassic deposits have increased thickness within the EHT
525 (Fig. 13). Maystrenko et al. (2005b) interpreted a Jurassic pulse of salt movement, which temporally
526 correlated with extension in the Lower Saxony Basin. Sedimentation in the Glückstadt Graben during
527 the Late Triassic was relatively high (Bachmann et al., 2008), so assuming that sedimentation during
528 deposition of the Keuper in the EHT exceeded or matched the accommodation space created by
529 subsiding salt, we can expect that the peripheral sinks of the Keuper unit were completely
530 synkinematically filled (Fig. 14a). Jurassic deposition without salt movement would then yield parallel
531 to subparallel layered strata affected by later erosion. Then we would expect that the present-day
532 remnants show no major local thickness variations (Fig. 14a). Therefore, the preserved Jurassic
533 depositional pattern indicates ongoing salt movement in the early Jurassic prior to erosion (Fig. 14b).

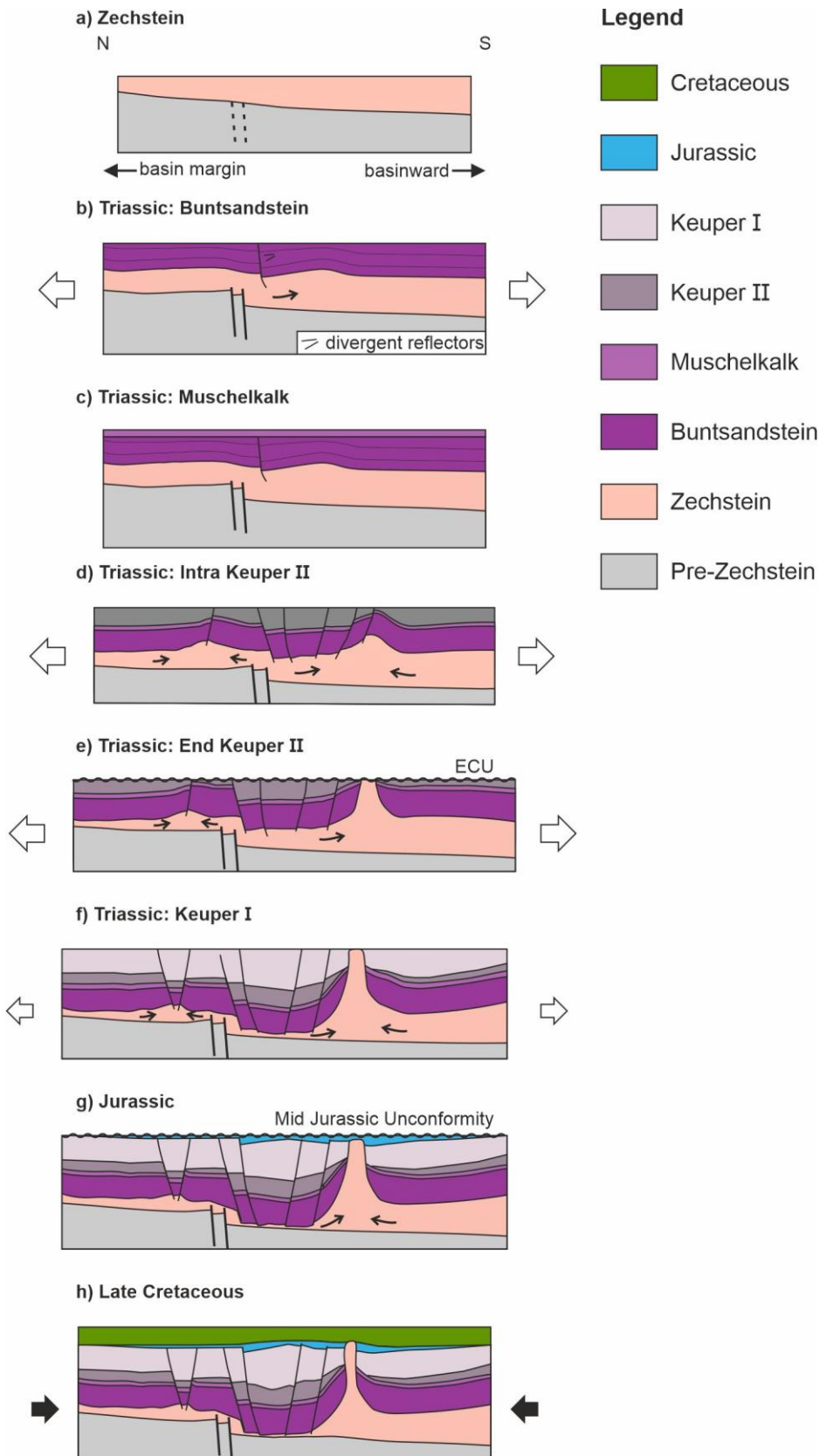


534

535 *Figure 14: Conceptual model assuming high sedimentation rate and syndepositional salt flow during deposition of the*
 536 *Keuper I followed by postkinematic deposition of the Lower Jurassic (A) and with ongoing salt movement in the early*
 537 *Jurassic (B). Model is based on the assumption that a high sedimentation rate during deposition of the Keuper I exceeded*
 538 *salt rise and thus, the peripheral sinks are completely filled with Keuper sediments. Black dashed line represents erosional*
 539 *surface due to the Mid Jurassic North Sea Doming event.*

540 5.2.2 Eastholstein-Mecklenburg Block

541 Within the Eastholstein-Mecklenburg Block (EHMB), local thickness variations of the Keuper II unit
 542 hardly correlate with the salt structures (Fig. 11). The crest of the “Fehmarn” salt pillow is slightly
 543 thinned, which could indicate the onset of minor salt movement. Overall, the Keuper II thickness
 544 within the EHMB shows the general thickening trend towards the south. During this time, salt
 545 movement seems to be restricted to the Eastholstein Trough, Kegnaes Diapir and Werre FZ, whereas
 546 the salt structures of the EHMB remained inactive. In much parts of the Bay of Kiel and above the
 547 crests of most salt structures, the top of the Keuper I unit is eroded. Thus, thickness variations of the
 548 Keuper I unit cannot be directly attributed to salt movement where the overlying Jurassic is
 549 completely missing (white line in Fig. 12). Northeast of the salt pillow “Trollegrund Nord”, increased
 550 thickness of the Keuper I unit and slightly divergent reflector suggests the beginning of salt
 551 movement and development of a small peripheral sink (Fig. 12) (Ahlrichs et al., 2020). The Jurassic in
 552 the EHMB is strongly affected by erosion and thicker remnants are only preserved at the flanks of salt
 553 structures (Fig. 13). In the absence of salt movement, we would expect Jurassic and Keuper I deposits
 554 to be horizontally layered without local thickness variations (Fig. 14a). Therefore, the pattern of
 555 erosion above the crest of salt structures and increased thickness of preserved remnants for the
 556 Keuper I (mostly Bay of Kiel) and Jurassic units, evidences salt movement prior to erosion (Fig. 14b).
 557 Based on the only minor indications for salt movement during deposition of the Keuper I in the Bay
 558 of Mecklenburg, we suppose that early Jurassic salt movement dominated in the EHMB. Hence, the
 559 onset of salt movement in the EHMB was considerably later than in the surrounding areas
 560 (Glückstadt Graben and northeastern basin margin). Therefore, the EHMB acted as a more stable
 561 transition zone between the Glückstadt Graben and the WPFS at the northeastern basin margin,
 562 whose development is controlled by tectonic movements along the Tornquist Zone (Krauss & Mayer,
 563 2004; Seidel et al., 2018).



597

598 *Figure 16: Conceptual model visualizing the proposed development of the Kegnaes Diapir. Diapiric breakthrough was*
 599 *accomplished by Late Triassic extension and erosion allowing piercement across the reduced overburden thickness at the*
 600 *basin margin.*

601 The Muschelkalk deposits show a relatively constant thickness, which suggests that the tectonic
 602 activity abated and salt flow decreased (Figs. 6b and 16c). During deposition of the Keuper II unit,

603 salt structure growth increased again indicated by the thick accumulation of Keuper II sediments
604 north of the diapir (Figs. 6b and 16d). This time marks the major phase of salt structure growth
605 during the pillow stage of the KD, which occurred under approx. E-W regional extension (Sørensen,
606 1998; Maystrenko et al., 2005b). Thereby, extension likely thinned the overburden of the salt
607 structure (Fig. 16d). At the flanks of the diapir, the Keuper II terminates in a toplap against the ECU
608 suggesting that Late Triassic erosion further affected the roof of the KD (Figs. 6b and 16e). Thus, we
609 interpret the ECU as the unroofing unconformity (Sørensen, 1998), which allowed piercing of the
610 overburden. Salt movement continued during deposition of the Keuper I unit with passive diapirism
611 and faulting within the overburden of the northern flank of the diapir (Fig. 16f). Preserved Jurassic
612 deposits are restricted to the overburden above the flanks north and south of the diapir (Fig. 6).
613 Following the same argumentation for the Jurassic as described in section 5.1.1, we interpret the
614 preservation of Jurassic deposits in the peripheral sinks of the KD as a sign of ongoing salt movement
615 during the Early Jurassic at least prior to Mid Jurassic erosion (Figs. 14 and 16g). The Cenomanian to
616 Santonian units do not show signs of syndepositional salt movement, which is in accordance with
617 findings from other salt structures in the study area (Ahlrichs et al., 2021). The narrow stem of the KD
618 suggests that the diapir was mildly squeezed (Fig. 16h, e.g.). This likely occurred during Late
619 Cretaceous inversion and is known from many other salt structures in the NGB (e.g. Kockel, 2003).

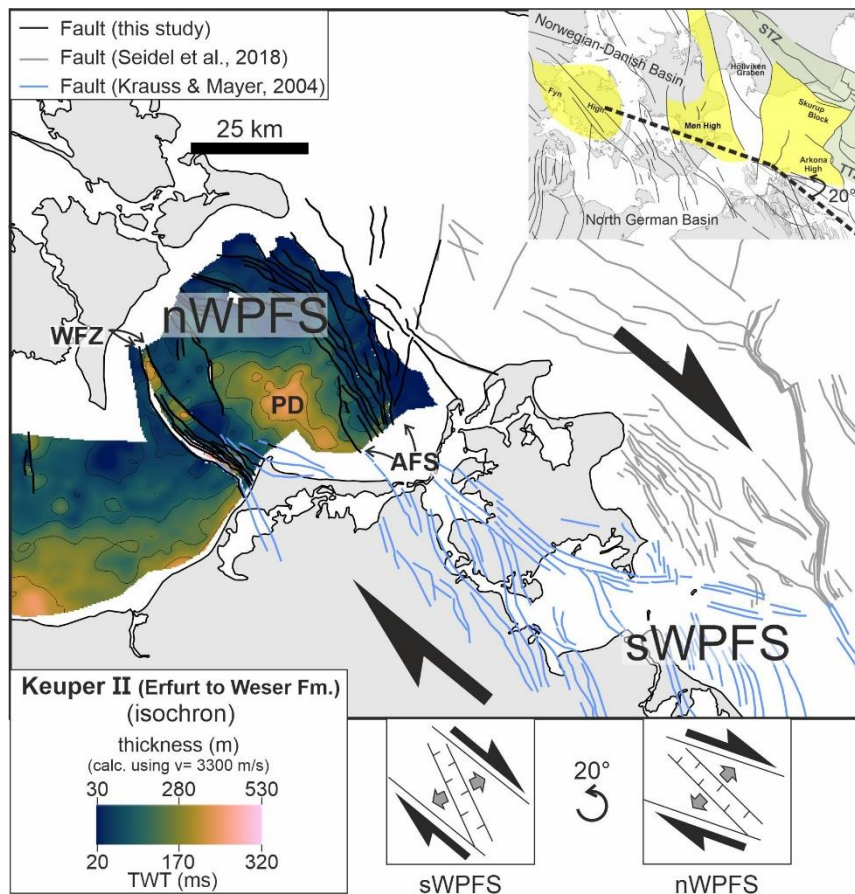
620 Based on the proposed structural evolution of the KD, the development of salt diapirs at the
621 northern basin margin was accomplished by reactive diapirism in combination with a reduced
622 overburden thickness by significant Late Triassic erosion. This allowed diapiric breakthrough by
623 extension and erosion and explains the isolated location of the KD and possibly of the other three
624 diapirs onshore Lolland at the northern basin margin. The absence of major Late Triassic erosion and
625 increased overburden thickness of the salt structures located within the Bays of Kiel and
626 Mecklenburg did not allow diapirism. Such initiation of diapirism is known from other parts of the
627 Southern Permian Basin, such as the Danish North Sea (Sørensen, 1998).

628 5.3 Faulting at the northeastern basin margin

629 Between the Werre FZ and Agricola FS, mapping of the Zechstein unit shows a local depression of the
630 base Zechstein, whose location coincides with a zone of increased thickness of the Buntsandstein,
631 Keuper and Jurassic successions (Figs. 8-9 and 11-13). The presence of this zone of increased
632 thickness is well known in the literature (Buntsandstein: Scheck & Bayer, 1999; Keuper and Jurassic:
633 Hansen et al., 2007; Hübscher et al., 2010; Deutschmann et al., 2018, the latter named this zone
634 "Prerow Depression" (PD)). The PD is part of a NW-SE oriented transtensional shear zone centered
635 around Rügen Island (Deutschmann et al., 2018; Seidel et al., 2018). During the Triassic – Early
636 Cretaceous, this area was affected by NW-SE dextral transtensional movements, which led to the
637 development of the Western Pomeranian Fault System (WPFS, Fig. 17) (Krauss & Mayer, 2004).
638 Faulting during deposition of the Keuper II unit in the Werre FZ and Agricola FS temporally correlate
639 with faulting in other regions of the WPFS during deposition of the Grabfeld Formation (Krauss &
640 Mayer, 2004; Beutler et al., 2012), and with E-W extension in the Glückstadt Graben (Figs. 7 and 11)
641 (Maystrenko et al., 2005b). During deposition of the Keuper I unit, faulting in the Werre FZ and
642 Agricola FS persisted (Fig. 12) (Ahlrichs et al., 2020). In this unit, the PD is more pronounced and
643 includes the entire area between the Werre FZ and Agricola FS suggesting ongoing subsidence (Fig.
644 12). Faults of the Werre FZ and Agricola FS remained active in the Jurassic (Hübscher et al., 2010;
645 Ahlrichs et al., 2020). The Jurassic deposits show a different pattern with a NE-SW elongated zone of
646 increased thickness, which further broadened and additionally included the area southwest of the
647 Werre FZ (Fig. 13).

648 In the southeastern part of the WPFS, the transtensional shear zone is characterized by numerous en
649 echelon faults and NW-SE striking grabens, which were formed in between the major fault zones (Fig.
650 17) (Seidel et al., 2018). Contrary, en echelon fault are absent in the northwestern part of the WPFS
651 and shearing was restricted to the faults of the bordering fault systems, while the area in between
652 subsided without being further faulted (Figs. 17 and 11 – 13). Notably, the thickness distribution of
653 the Keuper II unit suggests a 20° counterclockwise rotation of graben orientation compared to the
654 southeastern WPFS analyzed by Seidel et al. (2018) (Fig. 17). This rotation correlates with a change in
655 orientation of the basin margin from NW-SE southeast of Rügen Island towards a more WNW-ESE
656 trend along the Ringkøbing-Fyn High (dashed lines in the inset of Fig. 17). This suggests that the
657 development of the PD is influenced by the overall basin configuration and the deep-rooted
658 Paleozoic structures.

659 A possible explanation for the development of the PD would be rotational block faulting along deep-
660 seated Paleozoic faults, which were reactivated in the Triassic and early Jurassic. These deep-seated
661 faults have listric character and are detached near the top of the Paleozoic basement (Krawczyk et
662 al., 2002). During fault reactivation, the subsiding hanging walls possibly rotated creating locally
663 increased subsidence at the basin margin (Ahlrichs et al., 2020). However, the depositional pattern of
664 the Buntsandstein and Keuper II units contradict this explanation. Although, the elongated zone of
665 increased thickness of the Buntsandstein and Keuper II is located parallel to the basin margin, the
666 local depocenter occurs in the center between the Werre FZ and Agricola FS. Thus, the depocenter is
667 not directly adjacent to the basin marginal faults of the Agricola FS, where we would expect the
668 maximum subsidence of the hanging walls (Fig. 11). The depositional pattern fits better to the
669 development of a local transtensional sub-basin, bordered by the Agricola FS and Werre FZ (Fig. 17).
670 Interestingly, the location of the Keuper II depocenter within the PD correlates with the pinch-out of
671 mobile Zechstein units (Fig. 11). This could indicate that extensional stress localized here as it could
672 no longer be transferred within the detachment horizon, similar to the model suggested by Krawczyk
673 et al. (2002). A connection of the PD bordering faults to deeper Paleozoic structures is indicated by
674 the Late Triassic reactivation of the deep-rooted northern faults of the Agricola FS. The southwestern
675 border has a different character, as the Werre FZ is a thin-skinned fault system decoupled by the
676 Zechstein. An influence from deep-rooted structures seems likely but needs further investigations by
677 improved subsalt imaging in the area. Accordingly, this area marks the transition zone between thick-
678 skinned faulting at the basin margin and thin-skinned faulting decoupled by the Zechstein.



679

680 *Figure 17: Late Triassic reactivation of faults of the Western Pomeranian Fault System due to transtensional stress. Faults*
 681 *mapped in this study shown together with faults from Krauss and Mayer (2004); Seidel et al. (2018). The southern part of*
 682 *the Western Pomeranian Fault System (sWPFS) is characterized by an echelon fault and NW-SE striking grabens (Seidel et*
 683 *al., 2018). In the northern part of the Western Pomeranian Fault System (nWPFS), thickness of the Keuper II unit indicates a*
 684 *20° counterclockwise rotation of graben orientation correlating with a change in the orientation of the basin margin (dashed*
 685 *line in inset).*

686 5.4 Comparison with adjacent subbasins of the Southern Permian Basin

687 Generally, immature salt pillows dominate the peripheral part of the basin within our study area
 688 (Figs. 1 and 8). Salt welds are mostly absent. Mature salt walls and diapirs are almost exclusively
 689 located in the Glückstadt Graben apart from a few diapirs at the northern basin margin (Fig. 1). The
 690 distribution of salt pillows and more complex salt structures in adjacent basins is comparable (e.g.
 691 Polish Basin: Krzywiec, 2012; Dutch Basins: ten Veen et al., 2012; German North Sea: Kockel et al.,
 692 1995). In the Polish Basin, salt pillows dominate the peripheral region (Krzywiec, 2012). Similar to the
 693 Baltic sector of the NGB, sub-Zechstein faulting played a minor role in the development of these
 694 structures (Krzywiec, 2012). In the Dutch North Sea, major salt movement concentrates above
 695 basement faults in the basin center causing the development of salt diapirs and walls (ten Veen et al.,
 696 2012). Towards the peripheral region, minor salt movement occurred and only salt pillows are
 697 present (ten Veen et al., 2012). This is explained by less extension affecting the basin margin and
 698 platform highs during the Jurassic rifting (ten Veen et al., 2012). The development of the EHMB with
 699 its minor suprasalt deformation is very similar and likewise indicates that it experienced comparable
 700 less Triassic extension than the Glückstadt Graben. Interestingly, some salt diapirs developed along
 701 the platform edges within the Dutch North Sea basins, which were affected by Late Jurassic
 702 erosion (ten Veen et al., 2012). This could suggest a similar structural development as the Kegnaes
 703 Diapir in the Baltic Sea.

704 The initiation of salt structures during Keuper deposition within the Baltic sector of the NGB occurred
705 coeval with the initial formation of many salt structures in the peripheral parts of adjacent basins
706 (e.g. West Schleswig Block, onshore southeastern NGB, Terschelling Basin, Silver Pit Basin, Polish
707 Basin, see Fig. 5 of Warsitzka et al., 2019). While the triggering of salt movement in the basin center
708 and major rift grabens is mostly attributed to thick-skinned extension (e.g. Glückstadt Graben:
709 Maystrenko et al., 2005b, Horn Graben: Best et al., 1983, central Polish Basin: Krzywiec, 2012), a thin-
710 skinned trigger mechanism by either extension or gravity gliding is mostly discussed for the
711 peripheral regions (e.g. Cleaverbank Platform & Terschelling Basin: ten Veen et al., 2012, peripheral
712 Polish Basin: Krzywiec, 2012, see also overview map in Warsitzka et al., 2019). Therefore, the Triassic
713 initial formation of salt structures in the Baltic sector of the North German Basin by thin-skinned
714 extension fits well to triggering of salt movement in other peripheral parts of the Southern Permian
715 Basin. The base Zechstein in the study area is tilted by approx. 1° and has a thick overburden (Figs. 8-
716 13) (Ahlrichs et al., 2020). Clear indications for updip gravity-driven extension by basinward dipping
717 thin-skinned faults are absent suggesting that, if at all, gravity gliding played only a minor role (Fig. 8)
718 (see Ahlrichs et al., 2020 for a detailed discussion). Quantifying the true contribution of gravity
719 gliding to salt movement in less extended basins, by e.g. analogue modelling studies, is an aspect of
720 future work (Warsitzka et al., 2021). Overall, the formation of salt structures by thin-skinned
721 extension in the Baltic sector of the NGB can be well integrated with the transregional framework of
722 Triassic extensional tectonics in the Southern Permian Basin (e.g. Pharaoh et al., 2010). The West
723 Schleswig Block, which forms the western peripheral region of the Glückstadt Graben and thus, the
724 counterpart of the EHMB, represents an exception. Here, no tectonic trigger for salt movement has
725 been observed, which suggests salt tectonics due to differential loading (Warsitzka et al., 2019).
726 Future work comparing the development of the Glückstadt Graben and its marginal areas could
727 provide new insights into the triggering of salt movement in the West Schleswig Block.

728 6. Conclusions

729 We analyze the Triassic to Jurassic structural evolution of the Baltic sector of the North German Basin
730 using a dense network of high-resolution 2D seismic data tied to hydrocarbon and research wells.
731 Presented profiles and time-structure and isochron maps of the Zechstein, Buntsandstein,
732 Muschelkalk, Keuper II (Erfurt, Grabfeld, Stuttgart, Weser Formations), Keuper I (Arnstadt, Exeter
733 Formations) and Jurassic elucidate the Triassic-Jurassic structural evolution and salt movement of the
734 region. Mapping of the Zechstein unit revealed a previously unknown salt structure east of Als Island,
735 which we named “Als Øst”. The fault pattern of the study area is updated including a differentiation
736 between purely subsalt, thick-skinned faults and thin-skinned salt only affecting the suprasalt cover.
737 Thereby, the timing of salt movement and the transition from thick-skinned faulting at the basin
738 margin to deformation decoupled by the presence of thick Zechstein salt towards the basin center is
739 shown. This elucidates the development of salt structures in the context of regional tectonics within
740 an intracontinental sedimentary basin. Thick salt effectively decoupled basement deformation from
741 the suprasalt cover. Comparable minor regional extension caused the development of mostly
742 immature salt structures. The main conclusions are:

- 743 • At the northern basin margin, we observed first indications for salt movement and faulting at
744 the Kegnaes Diapir during deposition of the Buntsandstein. This early stage of faulting and
745 salt movement is in contrast with the common perception of quiet tectonic conditions
746 characterized by thermal subsidence based on the observations from other salt structures in
747 the study area, where the Buntsandstein and Muschelkalk were deposited prior to salt
748 movement (Figs. 6 and 9-10).

- 749 • Tectonic activity strongly increased in the Late Triassic during deposition of the Keuper II unit
750 including the onset of salt movement in the northeastern Glückstadt Graben, major salt
751 movement at the Kegnaes Diapir (reactive diapirism) and faulting at the northeastern basin
752 margin (Fig. 11).
- 753 • During deposition of the Keuper I and Lower Jurassic units, salt movement continued in the
754 northeastern Glückstadt Graben and at the Kegnaes Diapir (Figs. 12-13).
- 755 • We explain the development of salt diapirs at the northern basin margin based on the
756 development of the Kegnaes Diapir by reactive diapirism in combination with a reduced
757 overburden thickness by significant Late Triassic erosion. Thereby, the Kegnaes Diapir could
758 only pierce the overburden because of its location close to the basin margin, and thus
759 reduced overburden thickness when compared to other salt structures closer to the basin
760 center (Figs. 6 and 16).
- 761 • In the Triassic, the Eastholstein-Mecklenburg Block formed a more stable area at the
762 transition between the Glückstadt Graben and the fault systems of the northeastern basin
763 margin. Major faulting is absent and salt movement started only in the latest Triassic with its
764 dominant phase presumably in the early Jurassic (Fig. 15).
- 765 • We interpreted the thick accumulation of Keuper and Jurassic deposits west of Rügen
766 (Prerow Depression) as a transtensional sub-basin, bordered by the Agricola Fault System
767 and the Werre Fault Zone. In this area, Late Triassic extension induced transtensional
768 movements by a reactivation of deep-seated Paleozoic faults at the northeastern basin
769 margin. This caused increased subsidence of the Prerow Depression and corresponding
770 accumulation of Keuper and Jurassic deposits (Fig. 17).

771 Acknowledgements

772 We kindly acknowledge ExxonMobil Production Deutschland GmbH for providing the industry seismic
773 profiles and for the permission to publish the interpreted sections. We thank Emerson for providing
774 licenses of their software under the Paradigm University Research Program. This work is part of the
775 *StrucFlow* project and is a research and development study connected to the TUNB project by the
776 Federal Institute of Geosciences and Natural Resources (BGR) and the geological surveys of the
777 northern German federal states. The used scientific colourmap *batlow* prevents visual distortion and
778 exclusion of readers with colour vision deficiencies (Crameri et al., 2020).

779 *Data availability:* The seismic profile BGR16-221 of Fig. 7A, isochrone and time-structure maps shown
780 in this study are available in the supplementary material of this article. Further seismic data used for
781 mapping, is available from the authors and the Federal Institute for Geosciences and Natural
782 Resources (BGR) upon reasonable request. Industry seismic data available upon request at
783 ExxonMobil Production Deutschland GmbH.

784 *Author contributions:* Conceptualization of this study was done by NA, CH and VN. NA is the main and
785 corresponding author. NA carried out the seismic processing, seismic interpretation and mapping,
786 created the figures and was the primarily writer of the manuscript. Structural interpretation and
787 discussion of the results was done by NA, VN, CH and ES. All authors contributed to editing and
788 reviewing of the manuscript.

789 *Funding:* Gefördert durch die Deutsche Forschungsgemeinschaft (DFG) - 396852626/funded by the
790 Deutsche Forschungsgemeinschaft (DFG, German Research Foundation) - 396852626.

791 *Conflicts of interest:* The authors declare that they have no conflict of interest.

793 **References**

794 Ahlrichs, N., Hübscher, C., Noack, V., Schnabel, M., Damm, V., & Krawczyk, C. M. (2020). Structural
795 Evolution at the Northeast North German Basin Margin: From Initial Triassic Salt Movement
796 to Late Cretaceous-Cenozoic Remobilization. *Tectonics*, 39(7), 1-26.
797 <https://doi.org/10.1029/2019TC005927>

798 Ahlrichs, N., Noack, V., Hübscher, C., Seidel, E., Warwel, A., & Kley, J. (2021). Impact of Late
799 Cretaceous inversion and Cenozoic extension on salt structure growth in the Baltic sector of
800 the North German Basin. *Basin Research*, 34(1), 220-250. <https://doi.org/10.1111/bre.12617>

801 Al Hseinat, M., & Hübscher, C. (2014). Ice-load induced tectonics controlled tunnel valley evolution –
802 instances from the southwestern Baltic Sea. *Quaternary Science Reviews*, 97, 121-135.
803 <https://doi.org/10.1016/j.quascirev.2014.05.011>

804 Al Hseinat, M., & Hübscher, C. (2017). Late Cretaceous to recent tectonic evolution of the North
805 German Basin and the transition zone to the Baltic Shield/southwest Baltic Sea.
806 *Tectonophysics*, 708, 28-55. <https://doi.org/10.1016/j.tecto.2017.04.021>

807 Al Hseinat, M., Hübscher, C., Lang, J., Lüdmann, T., Ott, I., & Polom, U. (2016). Triassic to recent
808 tectonic evolution of a crestal collapse graben above a salt-cored anticline in the Glückstadt
809 Graben/North German Basin. *Tectonophysics*, 680, 50-66.
810 <https://doi.org/10.1016/j.tecto.2016.05.008>

811 Bachmann, G. H., Geluk, M., Warrington, G., Becker-Roman, A., Beutler, G., Hagdorn, H., Hounslow,
812 M., Nitsch, E., Röhling, H.-G., Simon, T., & Szulc, A. (2010). Triassic. In H. Doornenbal & A. G.
813 Stevenson (Eds.), *Petroleum Geological Atlas of the Southern Permian Basin Area* (pp. 149-
814 173). EAGE Publications.

815 Bachmann, G. H., Voigt, T., Bayer, U., von Eynatten, H., Legler, B., & Littke, R. (2008). Depositional
816 history and sedimentary cycles in the Central European Basin System. In R. Littke, U. Bayer,
817 D. Gajewski, & S. Nelskamp (Eds.), *Dynamics of complex intracontinental basins, the Central*
818 *European Basin System* (pp. 17-34). Springer Verlag. [https://doi.org/10.1007/978-3-540-](https://doi.org/10.1007/978-3-540-85085-4)
819 [85085-4](https://doi.org/10.1007/978-3-540-85085-4)

820 Baldschuhn, R., Binot, F., Fleig, S., & Kockel, F. (2001). Geotektonischer Atlas von Nordwest-
821 Deutschland und dem deutschen Nordsee Sektor [Bilingual digital atlas of the geotectonic
822 structure of Northwestern Germany and the German North Sea sector]. *Geologisches*
823 *Jahrbuch*, A(153), 1-88.

824 Berthelsen, A. (1992). Tectonic evolution of Europe. From Precambrian to Variscan Europe. In M. D.
825 Blum (Ed.), *A continent revealed: The European Geotraverse* (pp. 153-164). Cambridge
826 University Press.

827 Bertram, G. T., & Milton, N. J. (1989). Reconstructing basin evolution from sedimentary thickness; the
828 importance of palaeobathymetric control, with reference to the North Sea. *Basin Research*,
829 1, 247-257. <https://doi.org/10.1111/j.1365-2117.1988.tb00020.x>

830 Best, G., Kockel, F., & Schöneich, H. (1983). Geological History of the Southern Horn Graben. In J. P.
831 H. Kaasschieter & T. J. A. Reijers (Eds.), *Petroleum Geology of the Southeastern North Sea and*
832 *the Adjacent Onshore Areas: (The Hague, 1982)* (pp. 25-33). Springer Netherlands.
833 [10.1007/978-94-009-5532-5_2](https://doi.org/10.1007/978-94-009-5532-5_2)

834 Beutler, G., Junker, R., Niedieck, S., & Rößler, D. (2012). Tektonische Diskordanzen und tektonische
835 Zyklen im Mesozoikum Nordostdeutschlands. [Tectonic unconformities and tectonic cycles of
836 the Mesozoic in Northeastern Germany.]. *Zeitschrift der Deutschen Gesellschaft für*
837 *Geowissenschaften*, 163(4), 447-468. <http://dx.doi.org/10.1127/1860-1804/2012/0163-0447>

838 Beutler, G., & Schüler, F. (1978). Die altkimmerischen Bewegungen im Norden der DDR und ihre
839 regionale Bedeutung. *Zeitschrift für Geologische Wissenschaften*, 6, 403-420.

840 Bialas, J., Flueh, E. R., & Jokat, W. (1990). Seismic investigations of the Ringkøbing-Fyn High on
841 Langeland, Denmark. *Tectonophysics*, 176(1-2), 25-41. [https://doi.org/10.1016/0040-](https://doi.org/10.1016/0040-1951(90)90257-9)
842 [1951\(90\)90257-9](https://doi.org/10.1016/0040-1951(90)90257-9)

843 Brink, H., Dürschner, H., & Trappe, H. (1992). Some aspects of the late and post-Variscan
844 development of the Northwestern German Basin. *Tectonophysics*, 207(1), 65-95.
845 [https://doi.org/10.1016/0040-1951\(92\)90472-1](https://doi.org/10.1016/0040-1951(92)90472-1)

846 Clausen, O., & Pedersen, P. (1999). Late Triassic structural evolution of the southern margin of the
847 Ringkøbing-Fyn High, Denmark. *Marine and Petroleum Geology*, 16(7), 653-665.
848 [https://doi.org/10.1016/S0264-8172\(99\)00026-4](https://doi.org/10.1016/S0264-8172(99)00026-4)

849 Cramer, F., Shephard, G. E., & Heron, P. J. (2020). The misuse of colour in science communication.
850 *Nature Communications*, 11, 1-10. <https://doi.org/10.1038/s41467-020-19160-7>

851 Dadlez, R., & Marek, S. (1998). Major faults, salt- and non-salt anticlines. In R. Dadlez, S. Marek, & J.
852 Pokorski (Eds.), *Paleogeographic atlas of Epicontinental Permian and Mesozoic in Poland*
853 (1:2500000). Polish Geological Institute.

854 DEKORP-BASIN Research Group. (1999). Deep crustal structure of the Northeast German basin: New
855 DEKORP-BASIN '96 deep-profiling results. *Geology*, 27(1), 55-58.
856 [https://doi.org/10.1130/0091-7613\(1999\)027%3C0055:DCSOTN%3E2.3.CO;2](https://doi.org/10.1130/0091-7613(1999)027%3C0055:DCSOTN%3E2.3.CO;2)

857 Deutschmann, A., Meschede, M., & Obst, K. (2018). Fault system evolution in the Baltic Sea area west
858 of Rügen, NE Germany. *Geological Society, London, Special Publications*, 469(1), 83-98.
859 <https://doi.org/10.1144/sp469.24>

860 Drummon, B. J., Hobbs, R. W., & Goleby, B. R. (2004). The effects of out-of-plane seismic energy on
861 reflections in crustal-scale 2D seismic sections. *Tectonophysics*, 388(1-4), 213-224.
862 <https://doi.org/10.1016/j.tecto.2004.07.040>

863 Frahm, L., Hübscher, C., Warwel, A., Preine, J., & Huster, H. (2020). Misinterpretation of velocity pull-
864 ups caused by high-velocity infill of tunnel valleys in the southern Baltic Sea. *Near Surface*
865 *Geophysics*, 18(6), 643-657. <https://doi.org/10.1002/nsg.12122>

866 Frisch, U., & Kockel, F. (1999). Quantification of Early Cimmerian movements in NW-Germany.
867 *Zentralblatt für Geologie und Paläontologie, Teil 1*, 1-2, 571-600.

868 Gill, J., C. (2017). Geology and the Sustainable Development Goals. *Episodes - Journal of International*
869 *Geoscience*, 40(1), 70-76. <https://doi.org/10.18814/epiiugs/2017/v40i1/017010>

870 Guterch, A., Wybraniec, S., Grad, M., Chadwick, A., Krawczyk, C., Ziegler, P. A., Thybo, H., & De Vos,
871 W. (2010). Crustal structure and structural framework. In H. Doornenbal & A. Stevenson
872 (Eds.), *Petroleum Geological Atlas of the Southern Permian Basin Area* (pp. 11-23). EAGE
873 Publications.

874 Hakansson, E., & Pedersen, S. A. S. (1992). *Map of Bedrock Geology of Denmark*. Copenhagen, Varv
875 and Geological Survey of Denmark and Greenland.

876 Hansen, M. B., Lykke-Andersen, H., Dehghani, A., Gajewski, D., Hübscher, C., Olesen, M., &
877 Reicherter, K. (2005). The Mesozoic–Cenozoic structural framework of the Bay of Kiel area,
878 western Baltic Sea. *International Journal of Earth Sciences*, 94(5-6), 1070-1082.
879 <https://doi.org/10.1007/s00531-005-0001-6>

880 Hansen, M. B., Scheck-Wenderoth, M., Hübscher, C., Lykke-Andersen, H., Dehghani, A., Hell, B., &
881 Gajewski, D. (2007). Basin evolution of the northern part of the Northeast German Basin —
882 Insights from a 3D structural model. *Tectonophysics*, 437(1-4), 1-16.
883 <https://doi.org/10.1016/j.tecto.2007.01.010>

884 Hinsch, W. (1987). Lithology, Stratigraphy and Paleogeography of the Neogene in Schleswig-Holstein.
885 *Beiträge zur regionalen Geologie der Erde*, 18, 22-38.

886 Hoth, K., Rusbült, J., Zagora, K., Beer, H., & Hartmann, O. (1993). Die tiefen Bohrungen im
887 Zentralabschnitt der Mitteleuropäischen Senke - Dokumentation für den Zeitabschnitt 1962-
888 1990. *Verlag der Gesellschaft für Geologische Wissenschaften*, 2(7), 1-145.

889 Hübscher, C., Ahlrichs, N., Allum, G., Behrens, T., Bülow, J., Krawczyk, C., Damm, V., Demir, Ü., Engels,
890 M., Frahm, L., Grzyb, J., Hahn, B., Heyde, I., Juhlin, C., Knevels, K., Lange, G., Lydersen, I.,
891 Malinowski, M., Noack, V., . . . Stakemann, J. (2016). *MSM52 BalTec Cruise Report*.

892 Hübscher, C., Hansen, M. B., Triñanes, S. P., Lykke-Andersen, H., & Gajewski, D. (2010). Structure and
893 evolution of the Northeastern German Basin and its transition onto the Baltic Shield. *Marine*
894 *and Petroleum Geology*, 27(4), 923-938. <https://doi.org/10.1016/j.marpetgeo.2009.10.017>

895 Hübscher, C., Hseinat, M. a. A., Schneider, M., Betzler, C., & Eberli, G. (2019). Evolution of contourite
896 systems in the late Cretaceous Chalk Sea along the Tornquist Zone. *Sedimentology*, 66(4),
897 1341-1360. <https://doi.org/10.1111/sed.12564>

898 Hübscher, C., Lykke-Andersen, H., Hansen, M., & Reicherter, K. (2004). Investigating the structural
899 evolution of the western Baltic. *Eos*, 85(12), 115-115.
900 <https://doi.org/10.1029/2004EO120006>

901 Hudec, M. R., & Jackson, M. P. A. (2007). Terra infirma: Understanding salt tectonics. *Earth-Science*
902 *Reviews*, 82(1-2), 1-28. <https://doi.org/10.1016/j.earscirev.2007.01.001>

903 Huster, H., Hübscher, C., & Seidel, E. (2020). Impact of Late Cretaceous to Neogene plate tectonics
904 and Quaternary ice loads on supra-salt deposits at Eastern Glückstadt Graben, North German
905 Basin. *International Journal of Earth Sciences*, 109, 1029-1050.
906 <https://doi.org/10.1007/s00531-020-01850-8>

907 Jackson, M. P. A., & Hudec, M. R. (2017). *Salt Tectonics - Principles and Practice*. Cambridge
908 University Press. <https://doi.org/10.1017/9781139003988>

909 Japsen, P., Green, P. F., Bonow, J. M., & Erlström, M. (2015). Episodic burial and exhumation of the
910 southern Baltic Shield: Epeirogenic uplifts during and after break-up of Pangaea. *Gondwana*
911 *Research*, 35, 357-377. <https://doi.org/10.1016/j.gr.2015.06.005>

912 Japsen, P., Green, P. F., Nielsen, L. H., Rasmussen, E. S., & Bidstrup, T. (2007). Mesozoic-Cenozoic
913 exhumation events in the eastern North Sea Basin: a multi-disciplinary study based on
914 palaeothermal, palaeoburial, stratigraphic and seismic data. *Basin Research*, 19, 451-490.
915 <https://doi.org/10.1111/j.1365-2117.2007.00329.x>

916 Kammann, J., Hübscher, C., Boldreel, L. O., & Nielsen, L. (2016). High-resolution shear-wave seismics
917 across the Carlsberg Fault zone south of Copenhagen - Implications for linking Mesozoic and
918 late Pleistocene structures. *Tectonophysics*, 682, 56-64.
919 <https://doi.org/10.1016/j.tecto.2016.05.043>

920 Katzung, G. (2004). *Geologie von Mecklenburg-Vorpommern [Regional Geology of the State of*
921 *Mecklenburg-Western Pomerania, NE Germany]* (Vol. 1). E. Schweizerbart'sche
922 Verlagsbuchhandlung.

923 Kehle, R. O. (1988). The origin of salt structures. In B. C. Schreiber (Ed.), *Evaporites and Hydrocarbons*
924 (pp. 345-404). Columbia University Press.

925 Kley, J., & Voigt, T. (2008). Late Cretaceous intraplate thrusting in central Europe: Effect of Africa-
926 Iberia-Europe convergence, not Alpine collision. *Geology*, 36(11).
927 <https://doi.org/10.1130/g24930a.1>

928 Kockel, F. (2002). Rifting processes in NW-Germany and the German North Sea Sector. *Netherlands*
929 *Journal of Geosciences - Geologie en Mijnbouw*, 81(2), 149-158.
930 <https://doi.org/10.1017/S0016774600022381>

931 Kockel, F. (2003). Inversion structures in Central Europe - Expressions and reasons, an open
932 discussion. *Netherlands Journal of Geosciences - Geologie en Mijnbouw*, 82(4), 367-382.
933 <https://doi.org/10.1017/S0016774600020187>

934 Kockel, F., Baldschuhn, R., Best, G., Binot, F., Frisch, U., Gross, U., Jürgens, U., Röhling, H.-G., &
935 Sattler-Kosnikowski, S. (1995). *Structural and palaeogeographical Development of the*
936 *German North Sea Sector*. Schweizerbart Science Publishers.
937 http://www.schweizerbart.de//publications/detail/isbn/9783443110260/Kockel_Structural_and_Palaeogeographic

938

939 Kossow, D., & Krawczyk, C. M. (2002). Structure and quantification of processes controlling the
940 evolution of the inverted NE-German Basin. *Marine and Petroleum Geology*, 19(5), 601-618.
941 [https://doi.org/10.1016/S0264-8172\(02\)00032-6](https://doi.org/10.1016/S0264-8172(02)00032-6)

942 Krauss, M., & Mayer, P. (2004). The Vorpommern Fault System and its Regional Structural
943 Relationships to the Trans-European Fault. *Zeitschrift für Geologische Wissenschaften*, 32,
944 227-246.

945 Krawczyk, C., Eilts, F., Lassen, A., & Thybo, H. (2002). Seismic evidence of Caledonian deformed crust
946 and uppermost mantle structures in the northern part of the Trans-European Suture Zone,

947 SW Baltic Sea. *Tectonophysics*, 360(1-4), 215-244. <https://doi.org/10.1016/S0040->
948 [1951\(02\)00355-4](https://doi.org/10.1016/S0040-1951(02)00355-4)

949 Krzywiec, P. (2012). Mesozoic and Cenozoic evolution of salt structures within the Polish basin: An
950 overview. In G. I. Alsop, S. G. Archer, A. J. Hartley, N. T. Grant, & R. Hodgkinson (Eds.), *Salt*
951 *Tectonics, Sediments and Prospectivity, Special Publications* (pp. 381-394). The Geological
952 Society. <https://doi.org/10.1144/SP363.17>

953 Kuszniir, N. J., & Ziegler, P. A. (1992). The mechanics of continental extension and sedimentary basin
954 formation: A simple shear/pure-shear flexural cantilever model. *Tectonophysics*, 215(1-2),
955 117-131. [https://doi.org/10.1016/0040-1951\(92\)90077-J](https://doi.org/10.1016/0040-1951(92)90077-J)

956 Maystrenko, Y., Bayer, U., Brink, H.-J., & Littke, R. (2008). The Central European Basin System - an
957 Overview. In R. Littke, U. Bayer, D. Gajewski, & S. Nelskamp (Eds.), *Dynamics of complex*
958 *intracontinental basins, the Central European Basin System* (pp. 17-34). Springer Verlag.
959 <https://doi.org/10.1007/978-3-540-85085-4>

960 Maystrenko, Y., Bayer, U., & Scheck-Wenderoth, M. (2005a). The Glueckstadt Graben, a sedimentary
961 record between the North and Baltic Sea in north Central Europe. *Tectonophysics*, 397(1-2),
962 113-126. <https://doi.org/10.1016/j.tecto.2004.10.004>

963 Maystrenko, Y., Bayer, U., & Scheck-Wenderoth, M. (2005b). Structure and evolution of the
964 Glueckstadt Graben due to salt movements. *International Journal of Earth Sciences*, 94(5-6),
965 799-814. <https://doi.org/10.1007/s00531-005-0003-4>

966 Maystrenko, Y. P., & Scheck-Wenderoth, M. (2013). 3D lithosphere-scale density model of the
967 Central European Basin System and adjacent areas. *Tectonophysics*, 601, 53-77.
968 <https://doi.org/10.1016/j.tecto.2013.04.023>

969 Michelsen, O. (1978). Stratigraphy and distribution of Jurassic deposits of the Norwegian-Danish
970 Basin. *Danmarks Geologiske Underøgelse, Serie B(2)*, 1-28.

971 Nielsen, L. H., & Japsen, P. (1991). Deep wells in Denmark - 1935-1990. *Danmarks Geologiske*
972 *Undersøgelse, Serie A(31)*, 1-179.

973 Nöldecke, W., & Schwab, G. (1976). Zur tektonischen Entwicklung des Tafeldeckgebirges der
974 Norddeutsch-Polnischen Senke unter besonderer Berücksichtigung des Nordteils der DDR.
975 *Zeitschrift für Angewandte Geologie*, 23, 369-379.

976 Peacock, D. C. P., & Banks, G. J. (2020). Basement highs: Definitions, characterisation and origins.
977 *Basin Research*, 32, 1685-1710. <https://doi.org/10.1111/bre.12448>

978 Peryt, T. M., Geluk, M., Mathiesen, A., Paul, J., & Smith, K. (2010). Zechstein. In J. C. Doornenbal & A.
979 G. Stevenson (Eds.), *Petroleum Geological Atlas of the Southern Permian Basin Area* (pp. 123-
980 147). EAGE Publications.

981 Pharaoh, T., Duser, M., Geluk, M., Kockel, F., Krawczyk, C., Krzywiec, P., Scheck-Wenderoth, M.,
982 Thybo, H., Vejbaek, O. V., & van Wees, J.-D. (2010). Tectonic evolution. In H. Doornenbal & A.
983 G. Stevenson (Eds.), *Petroleum Geological Atlas of the Southern Permian Basin Area* (pp. 25-
984 57). EAGE Publications.

985 Rasmussen, E. S. (2009). Neogene inversion of the Central Graben and Ringkøbing-Fyn High,
986 Denmark. *Tectonophysics*, 465, 84-97. <https://doi.org/10.1016/j.tecto.2008.10.025>

987 Reinhold, K., Krull, P., Kockel, F., & Rätz, J. (2008). *Salzstrukturen Norddeutschlands: Geologische*
988 *Karte*. Hannover, Bundesanstalt für Geowissenschaften und Rohstoffe.

989 Rempel, H. (1992). Erdölgeologische bewertung der Arbeiten der Gemeinsamen Organisation
990 'Petrobaltic' im deutschen Schelfbereich [Evaluation of the petroleum geological work of the
991 consortium Petrobaltic in the German shelf area]. *Geologisches Jahrbuch, D99*, 3-32.

992 Scheck, M., & Bayer, U. (1999). Evolution of the Northeast German Basin - inferences from a 3D
993 structural model and subsidence analysis. *Tectonophysics*, 313, 145-169.
994 [https://doi.org/10.1016/S0040-1951\(99\)00194-8](https://doi.org/10.1016/S0040-1951(99)00194-8)

995 Schlüter, D., Jürgens, D., Best, G., Binot, F., & Stamme, H. (1997). *Analyse geologischer und*
996 *geophysikalischer Daten aus der südlichen Ostsee - Strukturatlas südliche Ostsee (SASO)*.

997 Schnabel, M., Noack, V., Ahlrichs, N., & Hübscher, C. (2021). A comprehensive model of seismic
998 velocities for the Bay of Mecklenburg (Baltic Sea) at the North German Basin margin -
999 implications for basin development. *Geo-Marine Letters*.

1000 Seidel, E. (2019). *The Tectonic Evolution of the German offshore area, as part of the Trans-European*
1001 *Suture zone (North and East of Rügen Island)* [Dissertation, University of Greifswald].
1002 Greifswald.

1003 Seidel, E., Meschede, M., & Obst, K. (2018). The Wiek Fault System east of Rügen Island: origin,
1004 tectonic phases and its relationship to the Trans-European Suture Zone. *Geological Society,*
1005 *London, Special Publications, 469*(1), 59-82. <https://doi.org/10.1144/sp469.10>

1006 Sirocko, F., Reicherter, K., Lehné, R., Hübscher, C., Winsemann, J., & Stackebrandt, W. (2008).
1007 Glaciation, salt and the present landscape. In R. Littke, U. Bayer, D. Gajewski, & S. Nelskamp
1008 (Eds.), *Dynamics of complex intracontinental basins, the Central European Basin System* (pp.
1009 233-245). Springer Verlag. <https://doi.org/10.1007/978-3-540-85085-4>

1010 Sørensen, K. (1986). Rim syncline volume estimation and salt diapirism. *Nature, 319*(2), 23-27.
1011 <https://doi.org/10.1038/319023a0>

1012 Sørensen, K. (1998). The salt pillow to diapir transition; evidence from unroofing unconformities in
1013 the Norwegian-Danish Basin. *Petroleum Geoscience, 4*, 193-202.
1014 <https://doi.org/10.1144/petgeo.4.3.193>

1015 STD 2016 (German Stratigraphic Commission, ed.; editing, coordination and layout: Menning, M., &
1016 Hendrich, A. (2016). Stratigraphic Table of Germany 2016. In. Potsdam: German Research
1017 Centre for Geosciences.

1018 Stewart, S. A., Harvey, M. J., Otto, S. C., & Weston, P. J. (1996). Influence of salt on fault geometry:
1019 examples from the UK salt basins. In G. I. Alsop, D. J. Blundell, & I. Davison (Eds.), *Salt*
1020 *Tectonics* (Vol. 100, pp. 175-202). Geological Society Special Publications.

1021 Strohmenger, C., Voigt, E., & Zimdars, J. (1996). Sequence stratigraphy and cyclic development of
1022 Basal Zechstein carbonate-evaporite deposits with emphasis on Zechstein 2 off-platform
1023 carbonates (Upper Permian, Northeast Germany). *Sedimentary Geology, 102*(1), 33 - 54.
1024 [https://doi.org/10.1016/0037-0738\(95\)00058-5](https://doi.org/10.1016/0037-0738(95)00058-5)

1025 ten Veen, J. H., van Gessel, S. F., & den Dulk, M. (2012). Thin- and thick-skinned salt tectonics in the
1026 Netherlands; a quantitative approach. *Netherlands Journal of Geosciences - Geologie en*
1027 *Mijnbouw, 91*(4), 447-464. 10.1017/S0016774600000330

1028 Thybo, H. (1997). Geophysical characteristics of the Tornquist Fan area, northwest Trans-European
1029 Suture Zone: indication of late Carboniferous to early Permian dextral transtension.
1030 *Geological Magazine, 134*(5), 597-606. <https://doi.org/10.1017/S0016756897007267>

1031 TUNB Working Group. (2021). *TUNB - Potenziale des unterirdischen Speicher- und Wirtschaftsraumes*
1032 *im Norddeutschen Becken*. Bundesanstalt für Geowissenschaften und Rohstoffe. Retrieved
1033 05.03.2021 from <https://gst.bgr.de/>

1034 Underhill, J. R., & Partington, M. A. (1993). Jurassic thermal doming and deflation in the North Sea:
1035 implications of the sequence stratigraphic evidence. *Geological Society, London, Petroleum*
1036 *Geology Conference series, 4*(1), 337-345. <https://doi.org/10.1144/0040337>

1037 Van Wees, J.-D., Stephenson, R., Ziegler, P. A., Bayer, U., McCann, T., Dadlez, R., Gaupp, R.,
1038 Narkiewicz, M., Bitzer, F., & Scheck, M. (2000). On the origin of the Southern Permian Basin,
1039 Central Europe. *Marine and Petroleum Geology, 17*(1), 43 - 59.
1040 [https://doi.org/10.1016/S0264-8172\(99\)00052-5](https://doi.org/10.1016/S0264-8172(99)00052-5)

1041 Vejbaek, O. V. (1997). Dybe strukturer i danske sedimentaere bassiner. *Geologisk Tidsskrift, 4*, 1-31.

1042 Vejbaek, O. V., Andersen, C., Dusar, M., Hergreen, W., Krabbe, H., Leszczynski, K., Lott, G. K.,
1043 Mutterlose, J., & van der Molen, A. S. (2010). Cretaceous. In J. C. Doornenbal & A. G.
1044 Stevenson (Eds.), *Petroleum Geological Atlas of the Southern Permian Basin Area* (pp. 195-
1045 209). EAGE Publications.

1046 Vendeville, B., & Jackson, M. P. A. (1992). The rise of diapirs during thin-skinned extension. *Marine*
1047 *and Petroleum Geology, 9*(4), 331 - 354. [https://doi.org/10.1016/0264-8172\(92\)90047-I](https://doi.org/10.1016/0264-8172(92)90047-I)

1048 Warren, J. (2008). Salt as sediment in the Central European Basin System as seen from a deep time
1049 perspective. In R. Littke, U. Bayer, D. Gajewski, & S. Nelskamp (Eds.), *Dynamics of complex*
1050 *intracontinental basins, the Central European Basin System* (pp. 249-276). Springer-Verlag.
1051 <https://doi.org/10.1007/978-3-540-85085-4>

- 1052 Warsitzka, M., Jähne-Klingberg, F., Kley, J., & Kukowski, N. (2019). The timing of salt structure growth
1053 in the Southern Permian Basin (Central Europe) and implications for basin dynamics. *Basin*
1054 *Research*, 31(2), 337-360. <https://doi.org/10.1111/bre.12323>
- 1055 Warsitzka, M., Kley, J., Jähne-Klingberg, F., & Kukowski, N. (2016). Dynamics of prolonged salt
1056 movement in the Glückstadt Graben (NW Germany) driven by tectonic and sedimentary
1057 processes. *International Journal of Earth Sciences*, 106(1), 131-155.
1058 <https://doi.org/10.1007/s00531-016-1306-3>
- 1059 Warsitzka, M., Kley, J., & Kukowski, N. (2013). Salt diapirism driven by differential loading — Some
1060 insights from analogue modelling. *Tectonophysics*, 591, 83-97.
1061 <https://doi.org/10.1016/j.tecto.2011.11.018>
- 1062 Warsitzka, M., Závada, P., Jähne-Klingberg, F., & Krzywiec, P. (2021). Contribution of gravity gliding in
1063 salt-bearing rift basins – a new experimental setup for simulating salt tectonics under the
1064 influence of sub-salt extension and tilting. *Solid Earth*, 12(8), 1987-2020. 10.5194/se-12-
1065 1987-2021
- 1066 Withjack, M. O., & Callaway, S. (2000). Active Normal Faulting Beneath a Salt Layer: An Experimental
1067 Study of Deformation Patterns in the Cover Sequence. *AAPG Bulletin*, 84(5), 627-651.
1068 <https://doi.org/10.1306/C9EBCE73-1735-11D7-8645000102C1865D>
- 1069 Ziegler, P. A. (1990a). *Geological Atlas of Western and Central Europe* (Vol. 2nd). Shell Internationale
1070 Petroleum Maatschappij B. V.
- 1071 Ziegler, P. A. (1990b). Tectonic and paleogeographic development of the North Sea Rift System. In D.
1072 Blundell & A. D. Gibbs (Eds.), *Tectonic Evolution of North Sea Rifts* (pp. 1-36). Oxford
1073 University Press.
- 1074 Zöllner, H., Reicherter, K., & Schikowsky, P. (2008). High-resolution seismic analysis of the coastal
1075 Mecklenburg Bay (North German Basin): the pre-Alpine evolution. *International Journal of*
1076 *Earth Sciences*, 97(5), 1013-1027. <https://doi.org/10.1007/s00531-007-0277-9>
- 1077